Masters Program in Geospatial Technologies

LiDAR-Derived Urban Morphology Indicators for Urban Heat Island Analysis

Lourenco Trindade Tavares de Oliveira Alexandre

Dissertation submitted in partial fulfilment of the requirements for the Degree of *Master of Science in Geospatial Technologies*

NOVA IMS Information Management School
Universitat Jaume I
Universität Münster

NOVA Information Management School
Instituto Superior de Estatística e Gestão de Informação
Universidade Nova de Lisboa

LiDAR-Derived Urban Morphology Indicators for Urban Heat Island Analysis

by

Lourenço Trindade Tavares de Oliveira Alexandre

Master Dissertation presented as partial requirement for obtaining the Master's Degree in Geospatial Technologies

Supervised by

Prof. Vicente de Azevedo Tang, PhD, NOVA Information Management School

Prof. Ana Cristina Marinho da Costa, PhD, NOVA Information Management School

Prof. Michael Gould, PhD, Universitat Jaume I

February, 2026

STATEMENT OF INTEGRITY

I declare that the work described in this document is my own and not from someone else. All the assistance I have received from other people is duly acknowledged and all the sources (published or not published) are referenced.
This work has not been previously evaluated or submitted to NOVA Information Management School or elsewhere. I further declare that I have fully acknowledged the Rules of Conduct and Code of Honor from the NOVA Information Management School.

Lisbon, 20 February 2026
Lourenço Trindade Tavares de Oliveira Alexandre

USE OF GENERATIVE ARTIFICIAL INTELLIGENCE

Tasks	NO	YES	Generative Artificial Intelligence tools
Better understand issues related to the research	x		
Summarizing text from bibliography / resources		x	ChatGPT-5.2
Summarizing the method(s) used	x		
Translating text	x		
Grammar check		x	ChaGPT-5.2
Paraphrase or rewriting text from other people / resources	x		
Coding in R, Python, etc.	x		
Get help on a software		x	ChaGPT-5.2
Creating and editing images, maps, videos, etc.	x		
Data analysis		x	Claude Sonnet -4.5
Specify below other tasks not mentioned above:			

ACKNOWLEDGMENTS

This dissertation represents not only the culmination of academic work, but also the support, encouragement, and guidance of many remarkable people to whom I am deeply grateful.

First, I would like to express my sincere appreciation to my thesis supervisor, Prof. Vicente de Azevedo Tang, for the constant guidance, insightful feedback, and unwavering support throughout this journey. Their knowledge, dedication, and encouragement were fundamental to the completion of this work.

I am also thankful to Prof. Marco Painho, coordinator of the Master's program, for fostering an inspiring academic environment and for continuously motivating students to strive for excellence. Their commitment greatly enriched this academic experience.

My deepest gratitude goes to my family. To my parents, Cristina Alexandre and Edgar Alexandre, thank you for your unconditional love, endless encouragement, and for always believing in me, even during the most challenging times. Your support has been my greatest strength. To my sibling, António Alexandre, and my cousin, Leonor Figueiredo, thank you for your constant presence, endless patience, and unwavering willingness to help whenever I needed it. Your support and encouragement have meant more to me than words can express.

I would also like to acknowledge my friends and colleagues who have accompanied me throughout my academic path. To those who have shared this journey from the very beginning, thank you for your companionship, collaboration, and friendship. A special note of appreciation to those who believed in my work and encouraged me to keep moving forward.

Finally, I would like to express my sincere gratitude for one of the greatest friendships this Master's degree has given me, Samuel Cabral. Thank you for your patience, understanding, and unwavering support throughout this entire journey. Your encouragement during the most demanding moments truly made all the difference.

To everyone who, in one way or another, contributed to this achievement, I extend my heartfelt thanks.

LiDAR-Derived Urban Morphology Indicators for Urban Heat Island Analysis

ABSTRACT

Urban Heat Island (UHI) intensity reflects complex interactions between urban form, surface characteristics, and atmospheric processes, which vary markedly between daytime and nighttime conditions. This study examines the extent to which two-dimensional and three-dimensional urban morphology indicators can explain the spatial variability of UHI intensity, with particular emphasis on diurnal dynamics. Satellite-derived land surface temperature data were combined with urban morphology indicators derived from remote sensing and LiDAR data, capturing both planar and volumetric characteristics of the built and vegetated environment. A machine learning framework based on LightGBM was employed to model daytime and nighttime UHI patterns separately, while SHAP-based explainable artificial intelligence techniques were used to interpret variable importance, non-linear responses, and context-dependent effects. The results show that urban morphology indicators capture meaningful and physically consistent spatial patterns of UHI intensity, particularly when three-dimensional structure is incorporated. However, their explanatory capacity is not uniform across the diurnal cycle. During daytime conditions, UHI variability is characterized by greater heterogeneity and non-linear behavior, reflecting the influence of radiative and surface–atmosphere interactions, which limits the explanatory power of static morphological descriptors. In contrast, nighttime UHI patterns exhibit more systematic relationships with indicators describing imperviousness and three-dimensional urban geometry, consistent with the dominance of heat storage and delayed release processes. Overall, the findings demonstrate that urban morphology functions as a conditional explanatory framework for UHI variability, whose relevance depends on the dominant physical processes and temporal context. While morphology-based indicators provide valuable structural insight, the results also highlight the importance of integrating temporal dynamics and complementary data sources to more fully capture urban thermal behavior

KEYWORDS

Urban Heat Island; Urban Morphology; LiDAR-derived Indicators; Diurnal Dynamics; Explainable Machine Learning

Sustainable Development Goals (SGD):

INDEX

INDEX OF TABLES

INDEX OF FIGURES

ACRONYMS

ABH – Average Building Height

ABV – Average Building Volume

ATH – Average Tree Height

BTA – Building Total Area

BR – Building Ratio

COS – Carta de Ocupação do Solo

DR – Density of Roads

DSM – Digital Surface Model

DTM – Digital Terrain Model

ISR – Impervious Surface Ratio

LAS – LASer Format file

LCZ – Local Climate Zone

LiDAR – Light Detection and Ranging

LightGBM – Light Gradient Boosting Machine

LOD – Level of Detail

LST – Land Surface Temperature

OSM – OpenStreetMap

RMSE – Root Mean Square Error

SLSTR – Sea and Land Surface Temperature Radiometer

SVF – Sky View Factor

SHAP – SHapley Additive exPlanations

SUHI / UHI – (Standardized) Urban Heat Island

1. INTRODUCTION

Urbanization has profoundly altered land surface characteristics and local energy balances, leading to systematic temperature differences between urban areas and their rural surroundings, a phenomenon commonly referred to as the Urban Heat Island (UHI). As cities expand and densify, natural surfaces are progressively replaced by impervious materials with high heat-storage capacity, while vegetation loss reduces evaporative cooling, resulting in elevated surface and air temperatures (Oke, 1982; Voogt & Oke, 2003). In the context of ongoing climate change, these processes intensify heat exposure in cities, amplifying thermal stress, increasing energy demand, and exacerbating public health risks during heatwave events (IPCC, 2023).

The magnitude and spatial configuration of UHI intensity are not uniform across urban areas. Instead, they reflect complex interactions between surface materials, atmospheric conditions, and the physical structure of the built environment (Arnfield, 2003). In particular, urban morphology, the three-dimensional arrangement of buildings, vegetation, and open spaces, plays a fundamental role in regulating radiative exchange, airflow, and heat storage within cities (Grimmond et al., 1999). Characteristics such as building height, density, sky-view factor, and vegetation structure influence how solar radiation is absorbed during the day and how stored heat is released at night, leading to pronounced diurnal contrasts in UHI behavior.

Despite extensive research on UHI processes, much of the existing literature has relied on two-dimensional representations of urban form derived from land-cover maps or optical imagery. While such approaches capture horizontal surface properties, they often fail to represent the vertical complexity of contemporary cities, limiting their ability to explain spatial variability in urban thermal patterns (Yan et al., 2015a). The increasing availability of airborne Light Detection and Ranging (LiDAR) data has enabled the direct quantification of three-dimensional urban morphology, allowing volumetric and height-based indicators to be derived with high spatial precision (Labetski et al., 2023a). These developments have opened new opportunities to better characterize the structural drivers of UHI intensity, particularly when combined with satellite-derived land surface temperature (LST) observations.

At the same time, the analytical frameworks used to relate urban morphology to UHI intensity have evolved. Traditional statistical models have provided valuable insights but are often constrained by linear assumptions and limited capacity to capture

interactions between morphological variables (Weng, 2009) .More recently, machine-learning approaches have demonstrated strong potential for modelling non-linear relationships between urban form and surface temperature patterns (Chakraborty & Lee, 2019). However, the interpretability of these models remains a critical challenge, especially in studies aiming to support urban planning and climate adaptation. Explainable artificial intelligence techniques, such as SHapley Additive exPlanations (SHAP), offer a means to reconcile predictive performance with transparent interpretation by explicitly quantifying the contribution of individual predictors to model outcomes.

An additional limitation in many UHI studies concerns the treatment of temporal variability. UHI intensity exhibits distinct daytime and nighttime dynamics, driven by different physical mechanisms. Daytime surface heating is largely controlled by solar radiation and surface properties, whereas nighttime UHI patterns are more strongly influenced by heat storage and delayed release from urban materials (Voogt & Oke, 2003) .Nevertheless, the extent to which urban morphology explains UHI variability across the diurnal cycle remains insufficiently explored, particularly using three-dimensional indicators and interpretable modelling frameworks.

In response to these gaps, this thesis examines how two-dimensional and three-dimensional urban morphology indicators contribute to explaining the spatial variability of UHI intensity under daytime and nighttime conditions. The research is guided by the following research questions:

- How do the spatial patterns of Urban Heat Island (UHI) intensity vary between daytime and nighttime conditions in Lisbon?
- To what extent do two-dimensional and three-dimensional urban morphology indicators contribute to explaining this variability in Lisbon?

The analysis is conducted using Lisbon as a case study. Lisbon provides a particularly relevant urban and climatic context, characterized by a Mediterranean climate with hot, dry summers (Peel et al., 2007), as well as a heterogeneous urban fabric. Despite growing research on UHI processes in European cities, an integrated framework combining high-resolution three-dimensional urban morphology indicators, machine-learning modelling, and explainable artificial intelligence techniques has not yet been applied in Lisbon. This limitation has been largely due to the recent public availability

of detailed airborne LiDAR data, released only last year. The availability of this data creates a timely opportunity to quantify the city's three-dimensional structure with high spatial precision. Applying this framework in Lisbon is especially important given the city's increasing exposure to extreme heat and the need for locally grounded evidence to inform climate adaptation and urban planning strategies.

To achieve the objectives of this study, satellite-derived land surface temperature data are integrated with urban morphology indicators derived from airborne LiDAR and ancillary geospatial datasets. A machine-learning framework based on the Light Gradient Boosting Machine (LightGBM) is employed to model UHI intensity separately for daytime and nighttime conditions. Explainable artificial intelligence techniques based on SHAP are subsequently applied to interpret variable importance and non-linear relationships. This integrated approach enables urban morphology to be analyzed not only as a predictive factor but also as an explanatory framework for urban thermal behavior.

By adopting this perspective, the thesis contributes to urban climate research by advancing the understanding of urban morphology as a conditional explanatory factor of Urban Heat Island variability, highlighting the role of temporal context in shaping surface thermal patterns. It demonstrates that the influence of urban form differs between daytime and nighttime thermal regimes. Methodologically, the thesis introduces an integrated framework that combines high-resolution three-dimensional urban data with interpretable machine-learning techniques, balancing predictive performance and model transparency while enabling future integration of complementary and dynamic data sources.

The remainder of this dissertation is organized as follows. Chapter 2 reviews the relevant literature on the Urban Heat Island phenomenon, urban morphology, remote sensing data, and analytical approaches. Chapter 3 describes the data sources, methodological framework, and modelling strategy adopted in this research. Chapter 4 presents and discusses the results, focusing on spatial UHI patterns and the contribution of urban morphology indicators under contrasting thermal regimes. Finally, Chapter 5 summarizes the main conclusions, discusses the limitations of the study, and outlines directions for future research.

2. LITERATURE REVIEW

Urbanization has transformed natural land cover with impervious materials, combined with increased anthropogenic heat emissions, leading to higher heat storage and reduced evaporative cooling in cities. Subsequent research expanded the concepts to incorporate atmospheric processes, radiative exchange, and the spatial variability of urban microclimates (Arnfield, 2003) while also refining the understanding of the specific conditions under which urban areas exhibit higher temperatures than their rural surroundings, emphasizing the role of surface structure and material properties (Voogt & Oke, 2003; Deilami et al., 2018).

To improve the comparability of UHI studies across cities, this review adopts the Local Climate Zone (LCZ) taxonomy, a standardized scheme that classifies urban and natural landscapes by quantifiable surface structure and cover (e.g., building height, imperviousness, vegetation fraction, sky-view factor). The LCZ framework enhances the reproducibility of urban–rural temperature contrasts and links thermal observations to urban form (Stewart & Oke, 2012) Details on how LCZ is operationalized in this review appear in later sections.

The advancements in Earth observation and geospatial technologies have ushered in a new era of urban climate research. The rapid development of satellite-based sensors, high-resolution imagery, and geographic information systems revolutionized how urban climate environments could be observed and analyzed (Voogt & Oke, 2003; Weng, 2009). Recent studies show that new satellite sensors and multi-sensor processing techniques have improved the precision of land-surface temperature (LST) and urban heat island intensity estimates derived from remote-sensing data.

This literature aims to synthesize theoretical, methodological, and empirical knowledge relevant to assessing the relationship between urban morphology and UHI intensity, providing the conceptual basis for the proposed workflow that integrates LiDAR-derived morphological indicators with remote sensing data and machine learning analysis. The review is organized as follows: Section (2.1) introduces the urban heat island phenomenon and its physical mechanisms; Section (2.2) examines the relationship between urban morphology and UHI; Section (2.3) reviews remote-sensing data and techniques for UHI analysis; Section (2.4) discusses morphological indicators and metrics derived from LiDAR and ancillary datasets; Section 2.6 explores modelling and analytical approaches used to interpret UHI

dynamics; and Section 2.7 identifies gaps in the literature that justify the present research.

2.2 URBAN HEAT ISLAND PHENOMENON

UHI has become one of the most pervasive and well-documented climatic phenomena. Through the pioneering climatological work of (Oke, 1982) which established a theoretical foundation by explaining how urbanization alters local energy exchanges through changes in surface materials, geometry, and human activity. Fundamentally, the UHI arises from alterations in the surface energy balance, represented by the equation $Q^* = QH + QE + \Delta QS + QF + QA$ (Voogt & Oke, 2003) where Q* is the net radiation, QH the sensible heat flux, QE the latent heat flux, ΔQS the heat stored in urban materials, QF the anthropogenic heat flux, and QA the horizontal heat advection. This formulation shows how urbanization alters the equilibrium between absorbed and released energy, increasing sensible heat and heat storage while reducing latent heat through the loss of vegetation and permeable surfaces, which collectively create imbalances.

Manifestations of the UHI phenomenon differ across different atmospheric layers and scales and are, overall, categorized into three types: surface, canopy, and boundary-layer heat islands. The surface UHI refers to the temperature difference between urban and rural environments, typically derived from satellite-based thermal infrared observations. The canopy-layer UHI describes the air temperature within the urban canopy, from ground level to the rooftop height, directly affecting human thermal comfort. The boundary layer, which extends above the city skyline into the lower atmosphere, can affect mesoscale climatic processes (Voogt & Oke, 2003; Deilami et al., 2018).

The UHI effect shows marked temporal variability, peaking at night under calm and clear-sky conditions when radiative cooling is limited by heat stored in urban materials and restricted air movement. During the day, surface UHIs dominate due to differential solar heating between impervious and vegetated surfaces, while nocturnal UHIs result mainly from the delayed release of stored heat (Oke, 1982). This diurnal asymmetry underscores the combined influence of surface properties, atmospheric conditions, and heat-storage processes.

It also varies spatially, since it is closely linked to the characteristics of local morphology, including building form, vegetation distribution, and surface material. Many empirical studies now control urban form using LCZ classes when designing measurements and comparisons (Park et al., 2017) This standardization facilitates consistent urban contrast and strengthens inferences about the drivers of UHI intensity.

The cumulative consequence of these processes is a persistent modification of the local microclimate, and understanding their physical, environmental, and morphological underpinnings is essential for interpreting urban thermal dynamics and the role of city form in shaping them.

2.2.1 URBAN HEAT ISLAND METRICS AND INDICES

Understanding the physical and morphological that affect UHI makes it quantification a central component of urban climate analysis. While previously, it was outlined the driving surface and canopy-layers UHIs, comprehending these dynamics empirically requires indices capable of translating thermal patterns into comparable metrics. These indices have become standard tools because they enable spatially explicit measurements consistent across time and urban contexts. Studies comparing urban–rural LST contrasts across cities (Imhoff et al., 2010) show that simple temperature differences can effectively characterize how development intensity shapes thermal environments. Other approaches extend this logic by incorporating spatial gradients or surface characteristics. For example, Schwarz et al. (2011) systematically compared several surface UHI metrics, illustrating how indicator choice influences the magnitude and temporal behavior of observed UHIs, yet confirming that all capture meaningful aspects of urban thermal contrast.

More refined indices were proposed to improve comparability and reduce the influence of absolute temperature variability. Normalized anomalies such as those used by Estoque et al. (2017a) quantify local departures from a city's background thermal field, producing an intensity measure less sensitive to seasonal fluctuations. Sobrino et al. (2013), used a similar approach of applying LST normalization within airborne thermal campaigns, which showed that standardized SUHI measures allow clearer separation between urban thermal signatures and naturally varying surface temperatures.

Beyond normalized indices, other commonly used measures include Gaussian-based UHI magnitudes (Streutker, 2002), hot-spot area indicators, or indices incorporating land-cover classes. Although these metrics differ in formulation, they share the goal of expressing the relative enhancement of surface temperatures caused by urbanization.

For this thesis, the selected UHI indicator, a normalized LST-based index, aligns with these methodological developments. Its formulation allows the dependent variable to express temperature intensity relative to local background conditions, reducing the influence of atmospheric variability while remaining sensitive to fine-scale morphological variation derived from LiDAR. As demonstrated in recent research (Han et al., 2025a), such indices are particularly suited for studies aiming to link three-dimensional urban form to spatial patterns of surface heating, thus providing a reliable and interpretable foundation for the analytical work that follows.

2.3 URBAN-MORPHOLOGY RELATIONSHIP

Urban Morphology has as important role in shaping the spatial and temporal dynamics of Urban Heat Island effect. It is understood as the three-dimensional arrangement of buildings, vegetation, and open spaces that govern how energy is absorbed, stored, and exchanged within the urban fabric. Xu et al. (2017a) explained that parameters such as building density, height, and sky-view factor directly modulate radiation trapping and airflow pathways, therefore controlling the spatial and temporal evolution of urban temperatures.

The influence of urban geometry on microclimate has been documented in different environmental context settings. In hot-arid climates, (Johansson, 2006) showed how narrow street canyons with high height-to-width ratios trap longwave radiation and restrict air movement, leading to significant nocturnal heat retention but providing shade that mitigates daytime heat stress. On the other hand, in humid tropical cities, Johansson and Emmanuel (2006) found that open street canyons with lower height-to-width ratios enhance sea-breeze penetration and convective cooling. Roth (2007) also synthesized findings from several (sub)tropical cities and concluded that the combined effects of geometry, vegetation, and surface moisture highly determine both the magnitude and timing of UHI formation.

These observations illustrate that the thermal response of urban form is inherently context dependent. Compact urban morphologies are generally associated with enhanced nocturnal heat retention due to reduced radiative loss, whereas the cooling potential of more open configurations depends strongly on surface characteristics and material properties. Understanding this morphological influence encompassed in the Local Climate Zone (LCZ) framework, we can better clarify the role of morphological typologies to determine thermal variability. As an example, (Matias & Lopes, 2024) confirmed this same conclusion, in Lisbon, where compact LCZ classes exhibited significantly higher land surface than the open or vegetated zones.

Regional studies have also revealed that morphological evolution interacts with broader climatic trends. In the Lisbon metropolitan area, (Silva et al., 2022) projected that future urban densification and reduced green cover will intensify nocturnal UHIs under warming climate scenarios, underscoring the cumulative impact of morphology and climate change. Comparable trends observed in Asian megacities suggest that vertical growth and land sealing amplify heat accumulation, particularly under stagnant atmospheric conditions (Meng et al., 2018)..

As these relationships vary across spatial scales and climatic contexts, their systematic assessment requires spatially explicit data capable of capturing both morphological diversity and surface temperature patterns. Geospatial Technologies now provide the means to quantify these interactions with increasing precision, forming the analytical foundation for the next stage of this review.

2.4 Remote Sensing Data for UHI Analysis

Remote sensing provides valuable data for a wide range of environmental and urban applications. According to Melesse et al. (2007) it serves as a crucial data source for hydrological modelling, watershed mapping, energy and water-flux estimation, fractional vegetation cover, impervious surface-area mapping, urban modelling, drought prediction and environmental monitoring. Among these, the retrieval has become particularly important for analyzing urban heat dynamics, as it enables the spatial assessment of surface energy balance and UHI intensity. Thermal remote sensing enables spatial mapping of surface heat distribution, yet its accuracy depends on emissivity correction, atmospheric compensation, and spatial resolution(Voogt & Oke, 2003).

Satellite sensors have progressively improved the precision and scope of UHI monitoring. As Tardy et al. (2016) traced the historical evolution of remote sensing technology from early meteorological satellites to modern multispectral missions such as Landsat, MODIS, ASTER, and Sentinel-3, also supporting the multi-sensor integration to enhance environmental and urban applications. This diversity enables combining optical, thermal, and airborne LiDAR data to examine both morphological and thermal dimensions of cities, an approach aligned with the methodology of this study using Sentinel-3 SLSTR for LST and LiDAR-derived morphological metrics.

Retrieving accurate LST still remains one of the main challenges in remote sensing. Li et al. (2013) offered a comprehensive synthesis of theoretical and algorithmic development grouping retrieval methods, according to their underlying principles and data requirements, all of which require careful atmospheric correction and emissivity estimations (Tardy et al., 2016). Other further studies redefined algorithms and developed automated workflows to improve consistency across sensors (Rozenstein et al., 2014). In parallel, satellite agencies established standardized data processing levels to ensure comparability between instruments and facilitate analysis. Satellite data are typically organized into successive processing levels, from radiometrically corrected measurements (Level-1) to derived geophysical variables (Level-2) and aggregated, analysis-ready products (Level-3) as explained in Nasa EarthData.

Not only are standardized data hierarchies essential for ensuring the consistency of satellite products, but ground-based temperature measurements are also valuable for validating them. It is widely recognized that cross-validation between Land Surface Temperature (LST) and near-surface air temperature enhances the reliability of Urban Heat Island (UHI) assessments, as demonstrated by Foissard et al. (2024), who employed dense in-situ networks for this purpose. Nevertheless, many studies have shown that LST, derived from thermal infrared sensors, provides a robust proxy for analyzing the spatial structure and intensity of surface UHIs (Sobrino et al., 2004). Unlike air temperature, which represents the thermal state of the atmosphere near the ground, LST reflects the radiative temperature of the land surface itself, directly influenced by material properties, vegetation, and urban morphology making it particularly suitable for correlation with LiDAR-derived morphological indicators in the subsequent analysis.

2.5 LiDAR for Urban Morphology Analysis

Light Detection and Ranging (LiDAR) is an active remote sensing technology that measures distances by emitting laser pulses and recording their return time to generate dense three-dimensional point clouds. A typical airborne LiDAR system integrates a laser scanner, Global Positioning System (GPS), and Inertial Measurement Unit (IMU) to compute both the spatial position and orientation of each laser pulse (Wehr & Lohr, 1999).When processed, the resulting point cloud can originate high-resolution Digital Elevation Models (DEMs) and Digital Surface Models (DSMs), capturing the natural and build structures with centimeter-level accuracy (Yuan, n.d.) LiDAR has the capacity to directly measure elevation and surface morphology, unlike passive optical sensors that infer such attributes indirectly, making it an essential technology for precise characterization of urban form and structure (Molua & Ataman, 2024a).

New LiDAR applications have fundamentally transformed how urban morphology is quantified and modelled. Traditional two-dimensional approaches relied on aerial imagery or land-use maps and these usually limited insight into the volumetric and vertical characteristics of cities (Yan et al., 2015) These constraints were overcome with LiDAR technology, since it enables a more complete three-dimensional reconstruction of the built environment by providing detailed measurements of height, volume and surface roughness. This transition has been underscored by Labetski et al. (2023b) who demonstrated how LiDAR data capture geometric complexity and anisotropy overlooked by footprint-based analyses. Similarly airborne LiDAR supports fine-scale modelling of solar radiation fields in dense urban cores, linking morphological structure to radiation availability.

More research has used LiDAR-derived indicators for predictive modelling. Recently, Chajaei and Bagheri (2024) integrated LiDAR-based morphological metrics into machine-learning framework for high-resolution air-temperature downscaling, which illustrated the potential of LiDAR bridging geometry with microclimate. Complementarily, (Shi et al., 2025) confirmed that morphological factors, especially built-up area ratio and patch configuration, are dominant nonlinear drivers of canopy-level temperature variations.

Its strength also lies in the ability to integrate with other key sensing practices such as hyperspectral, SAR, and optical data. Studies have shown that data fusion approaches

can significantly improve the identification of materials, vegetation and surface properties, which are critical for assessing urban energy balances and evapotranspiration processes (Kuras et al., 2021; Afroosheh & Askari, 2024). At operational scales, Molua and Ataman (2024) highlighted LiDAR's precision for infrastructure monitoring and deformation detection, while Salazar Miranda et al. (2022) applied terrestrial laser scanning to capture irregular morphologies in informal settlements, exemplifying its flexibility across diverse urban fabrics.

Although LiDAR has become an established tool in urban analysis, most existing frameworks that apply morphological indicators remain highly context specific. Methodological choices like point-cloud processing, spatial resolution, and metric aggregation are often tailored to study areas or research objectives, which limit cross-study comparability and reproducibility.

2.6 Morphological Indicators and Metrics

Morphological indicators are fundamental to understand and quantify urban morphology, so that spatial variations on the Urban Heat Island (UHI) effect are explainable. They describe the physical form and surface structure of the urban environment, which can help us provide measurable parameters that link the built form with the thermal behavior and energy exchanges within cities (Xu et al., 2017; Ren et al., 2011). These metrics allow a uniform and systematic comparison of urban structures across regions and from the basis for modeling microclimatic processes and mitigation strategies.

At the beginning, morphological indicators were predominantly two-dimensional, derived from planimetric datasets or remote sensing imagery. Commonly used parameters include the building coverage ratio (BCR), impervious surface fraction, vegetation indices such as NDVI, and pervious surface ratios, all of which directly influence surface temperature and heat retention (Zhao et al., 2019). Such parameters have been applied within the Local Climate Zone (LCZ) framework, which categorizes urban landscapes based on surface cover and structural characteristic (Stewart & Oke, 2012; Bechtel et al., 2016)

With modernization three-dimensional data acquisitions have introduced more detailed morphological metrics. Parameters such as mean building height, building volume density, frontal area index (FAI), sky view factor (SVF), and roughness length (z_0)

capture the vertical dimension of urban form, improving the representation of radiative trapping and wind flow dynamics (Grimmond et al., 1999; Han et al., 2025; Xu et al., 2017).Recent work emphasizes the value of integrating 3D indicators obtained from LiDAR and photogrammetric data to represent complex urban geometries that strongly affect cooling and convective exchange.

Efforts have been made to standardize morphological data thought global crowdsource initiatives such as World Urban Database and Access Portal Tools (WUDAPT; Efforts have been made to standardize morphological data thought global crowdsource initiatives such as World Urban Database and Access Portal Tools (WUDAPT; https://www.wudapt.org/), which promotes a consistent protocol for acquiring urban form and function data using freely available satellite imagery and open-source tools (Bechtel et al., 2016; Wang et al., 2018). Parallel to this, new emerging approaches now integrate multi-source datasets, machine learning, and digital-twin simulations to quantify the influence of morphological metrics on UHI intensity (Han et al., 2025b, Sukma et al., 2024). Explainable AI techniques, such as SHAP (Shapley Additive exPlanations) analysis, are increasingly applied to assess the relative contribution of indicators such as BCR, SVF, and vegetation fraction (Chajaei & Bagheri, 2024c;Han et al., 2025b). Nevertheless, challenges remain regarding data resolution, transferability between cities, and harmonization of 2D and 3D indicators for cross-regional assessments. Continued refinement of morphological metrics is essential for accurately modeling urban thermal behavior and informing climate-responsive urban design.

2.7 Modeling and Analytical Approaches

Quantitative modelling of urban heat processes has progressed through different methodological (generations), which reflects advances in theory, computation and data availability. At the beginning, urban climate research emphasized conceptual and semi-empirical representations of energy exchange (Oke, 1982) which later evolved into physically based and statistical frameworks capable of linking spatial form with thermal behavior.

The first numerical schemes represented urban canopy as a physical system governed by radiative convective fluxes. Parameterizations such as Town Energy Balance (TEB) model (Masson 2000) and subsequent developments like Building Effect

Parameterization (BEP) and Building Energy Model (BEM) introduced explicit treatment of building geometry, surface albedo, and anthropogenic heat within mesoscale climate models such as Weather Research and Forecasting – Uban Canopy Model (WRF-UCM).

In parallel, statistical and regression-based methods were developed to infer empirical relationships between morphological indicators and thermal patterns derived from remote sensing. Linear and multiple regression models demonstrated that parameters such as building density, vegetation fraction, and impervious surface ratio strongly influence land surface temperature (LST) (Weng, 2009; Zhao et al., 2019). To account for spatial heterogeneity, approaches such as Geographically Weighted Regression (GWR) and Spatial Error Models (SEM) were later adopted, revealing that the relative importance of morphological drivers varies with local context and scale (Niu et al., 2021; Ren et al., 2011). These techniques strengthened the interpretability of statistical modeling but remained constrained by linear assumptions and difficulties in capturing interactions among variables.

With the expansion of high-resolution Earth-observation data and computational capacity, machine-learning (ML) methods have become increasingly prevalent in UHI analysis. Algorithms such as Random Forests, Support Vector Machines, and Gradient-Boosting frameworks enable nonlinear modeling of multi-source datasets and have achieved superior performance in predicting LST and UHI intensity (Chakraborty & Lee, 2019; Zhou et al., 2018).

2.7.1 Explainable Machine Learning: LightGBM and SHAP

Among machine-learning approaches, gradient-boosting decision-tree models have become particularly influential because they capture complex nonlinear relationships between morphological variables and thermal patterns more effectively than classical regression techniques. LightGBM represents one of the most efficient implementations of this family, offering fast training, strong scalability, and high predictive accuracy (Ke et al., 2017.). Applications in geospatial and environmental modeling consistently show that LightGBM outperforms other ensemble learners such as Random Forests and XGBoost when dealing with large, high-dimensional datasets (Tanoori et al., 2024; Gaur & Deb, 2024). These characteristics make it well suited for integrating multi-

source urban morphology metrics, including LiDAR-derived indicators, into predictive frameworks for LST and UHI intensity.

Despite its predictive strength, LightGBM provides limited transparency, which can restrict its usefulness for urban climate interpretation and planning. This has motivated the integration of explainable-AI (XAI) techniques to clarify model behaviour. Recent studies, such as Chajaei & Bagheri (2024) and (Han et al., 2025b), demonstrate the value of SHAP for revealing how geometric and surface-cover variables modulate LST. By quantifying each feature's marginal contribution to predicted temperatures, SHAP enables more interpretable and policy-relevant insights. Such hybrid ML–XAI frameworks offer a robust basis for examining how LiDAR-derived morphological indicators influence UHI intensity, supporting both predictive accuracy and explanatory clarity in the modeling stages of this thesis.

Overall, modeling approaches to the UHI have evolved toward multi-scale, data-integrated, and interpretable frameworks. This progression, from physical energy-balance models to spatial regression, to explainable machine-learning systems—marks a broader shift in urban climate research: from demonstrating that cities are warmer, to understanding which specific morphological configurations drive these temperature patterns. This provides the conceptual foundation for combining LiDAR-based morphology and remote-sensing data in the analyses that follow.

2.8 Conclusion

In sum, the literature demonstrates that urban thermal patterns emerge from the combined effects of surface energy processes, urban morphology, and the spatial structure of the built environment (Oke, 1982; Voogt & Oke, 2003). Remote-sensing advances have enabled increasingly precise retrieval of land-surface temperature and urban form, expanding the scope of UHI research from broad urban–rural comparisons to fine-scale morphological analyses (Weng, 2009; Li et al., 2013). At the same time, LiDAR and other 3D datasets have made it possible to quantify the geometric and volumetric properties that shape radiative trapping and airflow within cities (Yan et al., 2015; Labetski et al., 2023).

Across these developments, the literature consistently shows that urban morphological characteristics, such as building height, density, sky-view factor, and vegetation structure, play a significant role in shaping surface thermal patterns, even if their

influence varies with local context, scale, and environmental conditions (Xu et al., 2017; Matias & Lopes, 2024). Correspondingly, the choice of UHI metric significantly influences how these relationships are detected, with normalized LST-based indicators offering improved comparability across space and time (Estoque et al., 2017; Sobrino et al., 2013).

Methodologically, the field has shifted from physically based energy-balance models toward data-driven approaches capable of capturing nonlinear interactions between morphology and temperature (Chakraborty & Lee, 2019; Zhou et al., 2018). Gradient-boosting frameworks, particularly LightGBM, now provide state-of-the-art predictive capacity for geospatial thermal modelling (Ke et al., 2017), while explainable-AI techniques such as SHAP offer a means to recover interpretability without sacrificing performance (Chajaei & Bagheri, 2024; Han et al., 2025).

Collectively, the literature underscores the importance of integrated, interpretable, and multi-source approaches for understanding urban heat dynamics. At the same time, previous studies emphasize that morphology–temperature relationships are shaped by environmental and structural variability across cities (Arnfield, 2003; Zhou et al., 2018). Within this evolving methodological landscape, extending these approaches to additional urban contexts allows their transferability and context sensitivity to be more systematically assessed. In Lisbon, research has examined UHI dynamics and morphological typologies (Matias & Lopes, 2024; Silva et al., 2022), providing valuable insight into the city's thermal structure. However, the integration of LiDAR-derived three-dimensional indicators within an explainable machine-learning framework has not yet been systematically assessed in this context, despite the growing application of similar approaches in other urban environments. Situating the present study within this methodological trajectory allows these established approaches to be evaluated under the specific morphological and climatic conditions of Lisbon, thereby contributing to the broader comparative understanding of urban morphology–UHI relationships.

3. METHODOLOGY

This chapter outlines the set of procedures adopted to analyze the relationship between urban morphological characteristics and land surface temperature (LST) within the study area (Figure 1). The workflow comprises four main stages: (i) acquisition and preparation of multisource geospatial data, (ii) derivation of LiDAR-based morphological indicators, (iii) extraction and harmonization of thermal information from Sentinel-3 imagery, and (iv) modelling and interpretation of the links between urban form and surface temperature.

The overall methodological framework was inspired by recent advances in the analysis of Urban Heat Island dynamics from a three-dimensional urban morphology perspective, particularly the work of Han et al. (2025b).While the present study adopts a similar conceptual structure, integrating multi-source geospatial data, 2D and 3D urban morphology indicators, and explainable machine learning, the specific data sources, spatial scale, indicator definitions, and processing workflows were adapted to the characteristics of the study area and research objectives. This ensures methodological consistency with established approaches while allowing flexibility to address local urban conditions and data availability.

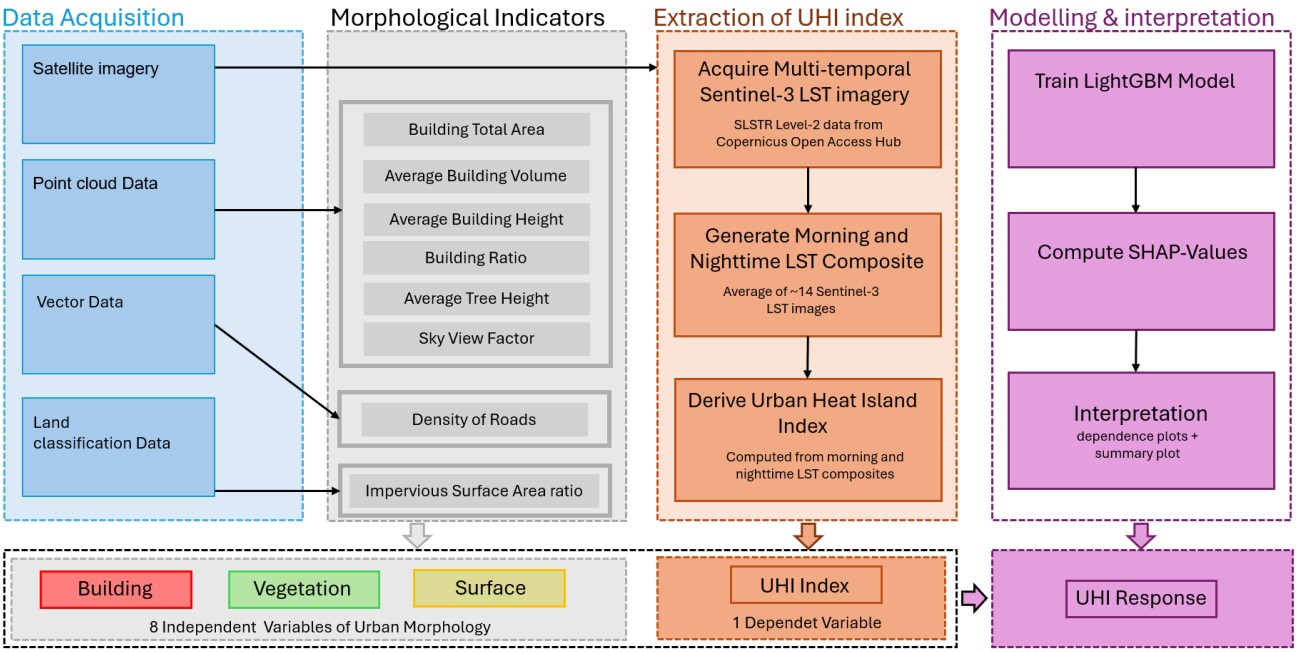

Figure 1 : Methodological workflow diagram

3.1 DATA SOURCES

This study integrates multiple geospatial datasets to analyze the spatial patterns of urban heat during the summer period of 2024. The datasets were selected based on their spatial resolution, temporal coverage, and ability to support the calculation of urban morphology indicators. The following subsections describe each dataset, its characteristics, and the justification for its inclusion in this research

3.1.1 SENTINEL-3 (SLSTR) THERMAL IMAGERY

The thermal data were obtained from the Sea and Land Surface Temperature Radiometer (SLSTR) onboard the Sentinel-3 satellites and downloaded from the Copernicus Open Access Hub. This study used the Land Surface Temperature (LST) Level 2 product, which includes all required radiometric, angular, and atmospheric corrections. Only observations from June, July, and August 2024 were used to ensure temporal consistency with the airborne LiDAR acquisition conducted in July 2024, minimizing potential mismatches between the mapped urban morphology and the analyzed thermal conditions.

To maintain a balanced temporal sampling across the season, a fixed weekly structure was adopted (days 1–6, 7–13, 14–20, 21–27, and 28–30/31). This approach allowed the selection of one daytime and one night-time image per interval whenever valid acquisitions (when cloud-cover percentage was below 20%). A summary of the number of selected images per month, according to this selection strategy, is presented in Table 1. SLSTR's spatial resolution of approximately 1 km is suitable for analyzing mesoscale thermal patterns and for subsequent integration with the grid used to derive urban morphology indicators.

Table 1 : Satellite imagery selection

Month (2024)	Number of Weeks Considered	Images Selected per Week	Cloud-Cover Threshold	Total Images
June	4	2 (day + night)	< 20%	8
July	5	2 (day + night)	< 20%	10
August	5	2 (day + night)	< 20%	10

3.1.2 LiDAR Point Cloud Data

The second major dataset used in this study consists of a high-resolution airborne LiDAR point cloud, obtained from the DGT (Direção-Geral do Território) through its open data platform. The DGT is the Portuguese national authority responsible for the production, management and dissemination of official geographic and cartographic information. The dataset was previously geometrically corrected and provided with a comprehensive classification scheme that differentiates terrain, built structures, vegetation, water bodies and other surface elements. The full list of classes and their descriptions is presented in Table 2. Each LiDAR point includes XYZ coordinates, RGB and NIR reflectance, and intensity, enabling detailed geometric and radiometric analysis.

Table 2 : Point cloud classification

Class Code	Class Name	Description
1	Other	Points that do not belong to any specific semantic class (unclassified).
2	Ground	Bare earth / terrain points used for DTM generation and ground-based indicators.
3	Low Vegetation	Vegetation with low height (typically < 1 m).
4	Medium Vegetation	Vegetation of intermediate height.
5	High Vegetation	Tall vegetation such as mature trees.
6	Buildings	Points corresponding to rooftops and other built structures.
7	Noise	Erroneous returns or artefacts detected during classification.
9	Water	Points classified as water bodies.
26	Bridges	Points corresponding to bridge structures.

3.1.3 OPENSTREETMAP (OSM) DATA

The road network dataset (figure 2) was obtained from OpenStreetMap (OSM) via the Geofabrik (https://www.openstreetmap.org) download service, which provides regional extracts in Shapefile format. The selected extract corresponds to Lisbon's administrative division and includes all mapped transportation features within the study area. OSM data are openly licensed and show high completeness for transportation networks in dense urban environments such as Lisbon. The dataset serves as the basis for deriving road-related morphological indicators.

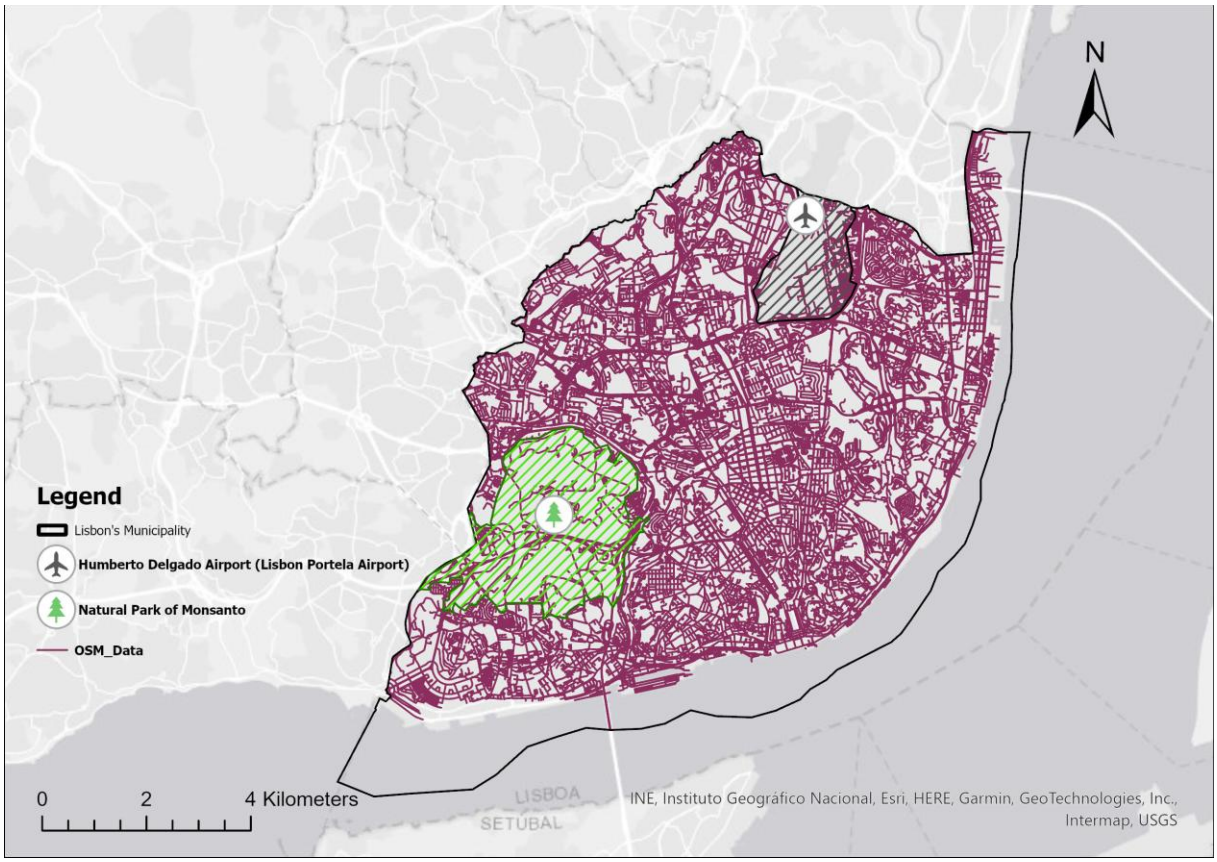

Figure 2 : OSM road network data

3.1.4 LAND COVER DATASET

The land classification dataset (figure 3) used in this study corresponds to the Portuguese Carta de Ocupação do Solo (COS), produced by the Direção-Geral do Território (DGT) in 2025. The COS provides a hierarchical thematic classification of land-use and land-cover types at 10 m spatial resolution.

The dataset includes detailed information on artificial and natural land-cover categories and was used to support the identification of impervious and pervious surfaces within the study area.

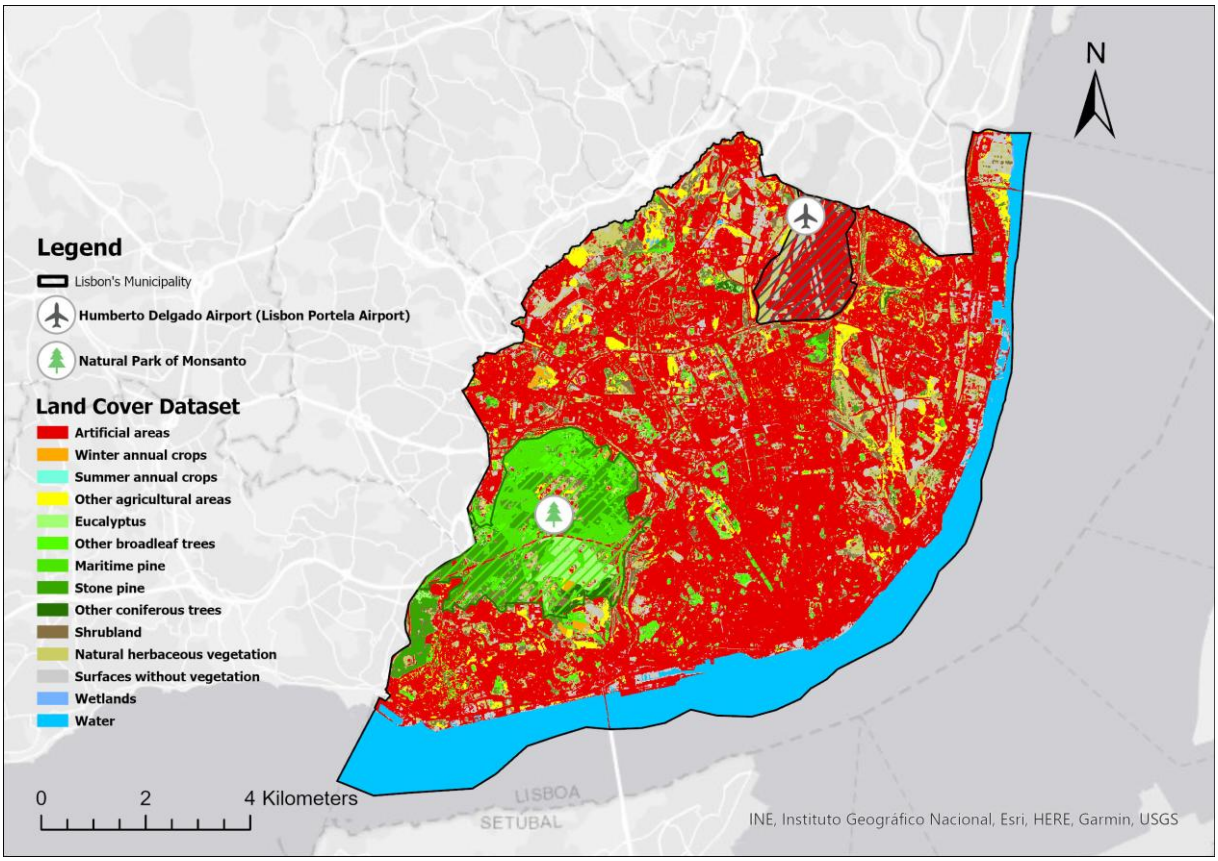

Figure 3 : Land cover dataset

3.2 CONSTRUCTION OF THE ANALYTICAL GRID

To ensure spatial consistency across datasets with different resolutions and acquisition geometries, all analyses were performed on a common 1 km × 1 km analytical grid (Figure 4). The grid was derived from a cloud-free Sentinel-3 SLSTR LST scene acquired on 2 July 2024 at 10:00 UTC, which offered the most complete spatial

coverage over the study area. Using this scene as reference ensured alignment with the native SLSTR pixel footprint, avoiding any resampling of the dependent variable that could introduce smoothing or artefacts (Han et al., 2025b).

The grid was generated in the national projected coordinate system ETRS89 / PT-TM06 (EPSG:3763) and subsequently clipped to the administrative boundary of the Municipality of Lisbon.

The final grid contains 77 tiles, each representing an independent spatial unit for integrating LST-derived UHI values and computed urban morphology indicators.

Defining the grid from the structure of the SLSTR data ensured that all variables, ranging from meter-scale LiDAR indicators to kilometer-scale thermal observations, were normalized into comparable areal units. This design minimized scale inconsistencies and provided a stable spatial framework for the subsequent machine learning analysis.

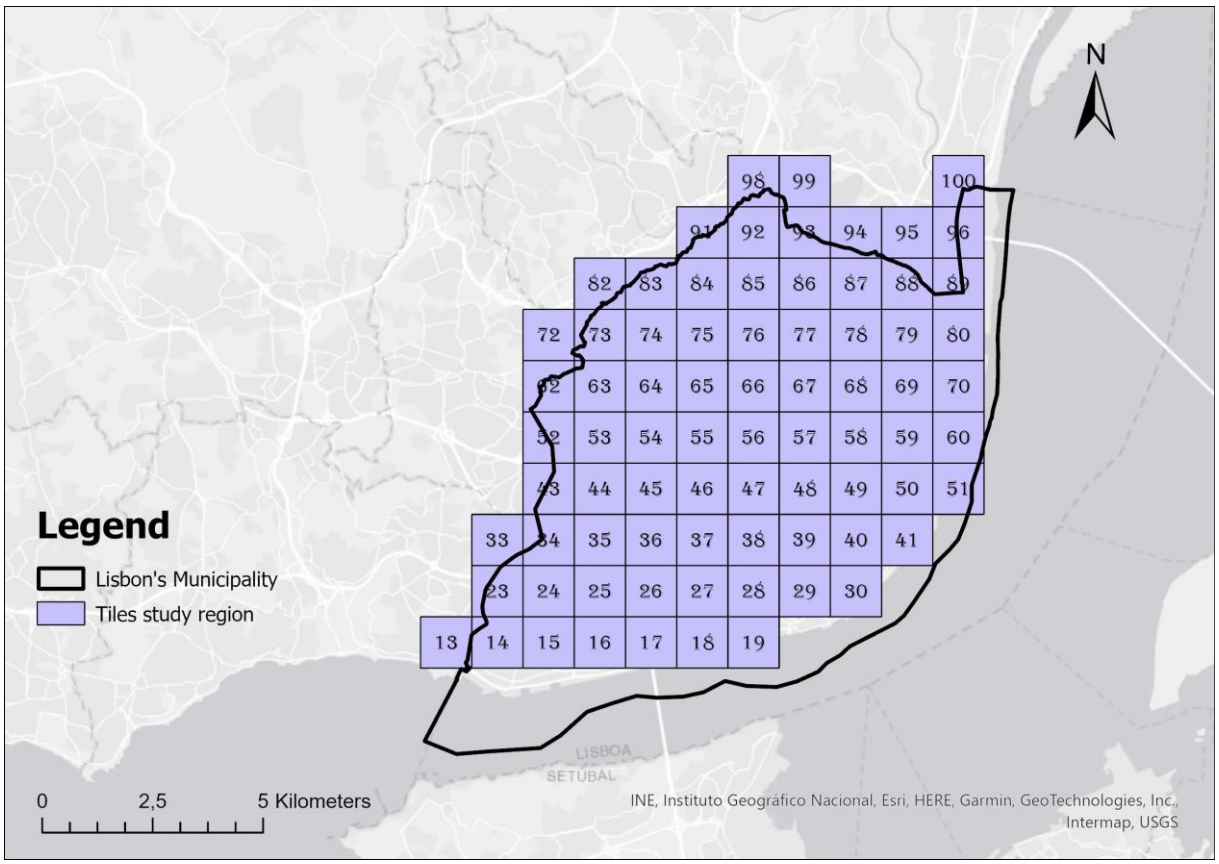

Figure 4 : Study Region Analytical Grid

3.3 Pre-processing Workflow

The different datasets used in this study: Sentinel-3 thermal imagery, LiDAR point-cloud data, land-cover information (COS), and OpenStreetMap (OSM) vector layers, possess distinct spatial resolutions, coordinate systems, and geometric structures.

To allow their integration into a unified analytical framework, a pre-processing workflow was developed to harmonize all datasets (Figure 5) before the extraction of morphological indicators and the Urban Heat Island (UHI) index.

As previously mentioned in Section **3.2** all datasets were aligned to a common 1 km × 1 km grid derived from a reference Sentinel-3 LST scene. This grid acts as the spatial unit of analysis, ensuring that both dependent (LST-based UHI) and independent (morphological indicators) variables refer to the same spatial units.

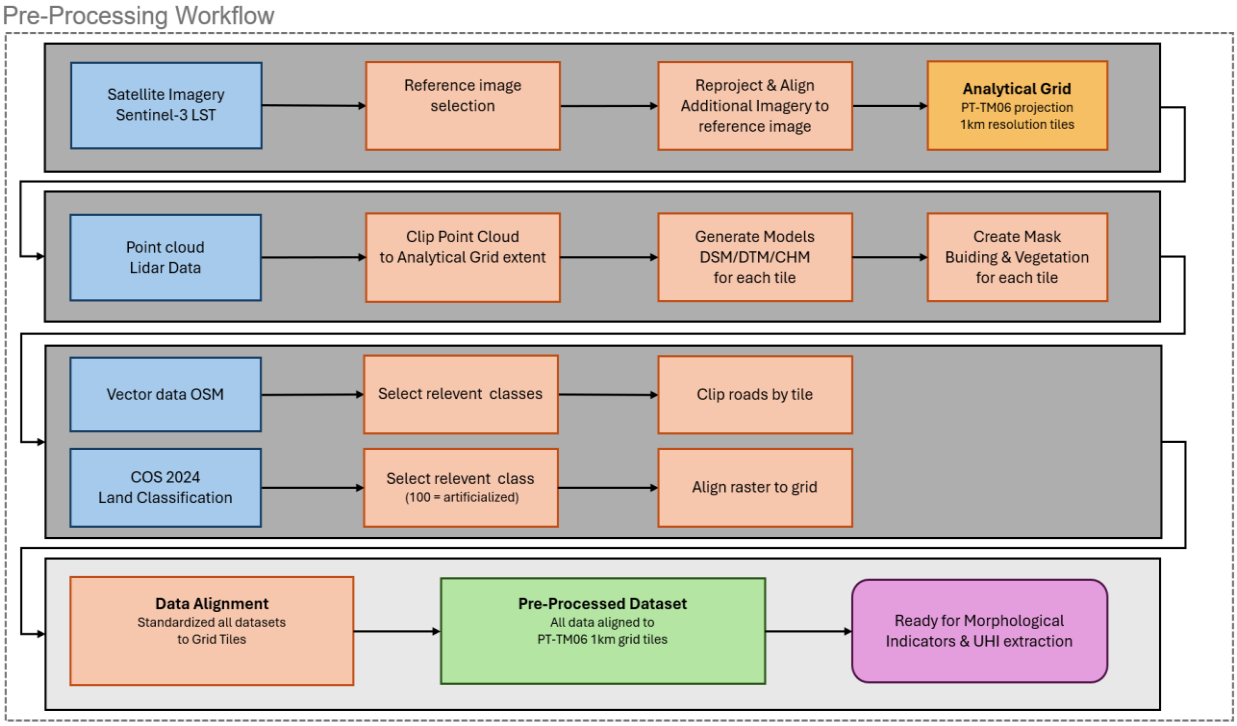

Figure 5 : Pre-processing workflow

LiDAR point-cloud Data

Because the original LiDAR tiling scheme did not align with the analytical grid, the individual LAS files were merged into a single dataset before being clipped to the municipal extent. The resulting point cloud was used to derive the Digital Terrain Model (DTM), Digital Surface Model (DSM), Canopy Height Model (CHM), and building and vegetation masks, preserving geometric detail while ensuring compatibility with the grid structure.

Vector layers from OpenStreetMap

The OSM dataset was used to extract the municipal road network. Only road categories consistently mapped across the municipality (motorway, trunk, primary, secondary, tertiary, residential, and service) were retained for analysis. The selected features were reprojected to ETRS89 / PT-TM06 (EPSG:3763), clipped to the analytical grid, and processed to quantify road-segment lengths within each spatial unit. These measurements supported the computation of road-density indicators, including the Building Ratio (BR).

COS 2024 land-classification dataset

Land classification dataset was used to identify impervious surfaces. From this dataset, only class *100 – Artificialized Areas* was extracted and aligned to the grid resolution. This raster layer provided the basis for calculating the Impervious Surface Area Ratio in combination with specific LiDAR-derived classes.

3.4 Urban Morphology Indicator Computation

Urban morphology indicators quantify the structural and functional characteristics of the built and natural environment within each grid tile. Table 3 summarizes the full set of 2D and 3D indicators considered in this study, adapted from the framework proposed by Han et al. (2025). Each indicator was computed directly on the 1 km × 1 km analytical grid, to avoid unnecessary spatial transformations and to maintain consistency with the native scale of the Sentinel-3 thermal observations.

Table 3: Morphological Indicators Considered

Indicator	Acronym	Description	Formula	Type
Building Total Area	**BTA**	Total footprint area of all buildings within a grid cell.	$BTA = \sum_{i=1}^{n_b} A_i^b$	**2D**
Density of Roads	**DR**	Road length per grid cell area.	$DR = \frac{L_{road}}{A_{grid}}$	**2D**
Impervious Surface Ratio	**ISR**	Proportion of impervious surface within the grid cell.	$ISR = \frac{A_{imp}}{A_{val}}$	**2D**
Building Ratio	**BR**	Ratio between building-class points and ground-class points.	$BR = \frac{Num_b}{Num_g}$	**3D**
Average Building Height	**ABH**	Mean height of buildings within the grid cell.	$ABH = \frac{1}{n_b} \sum_{i=1}^{n_b} H_i^b$	**3D**
Average Building Volume	**ABV**	Mean building volume within the grid cell.	$ABV = \frac{1}{n_b} \sum_{i=1}^{n_b} V_i^b$	**3D**
Average Tree Height	**ATH**	Mean tree height within the grid cell.	$ATH = \frac{1}{n_t} \sum_{i=1}^{n_t} H_i^{t,}$	**3D**
Sky View Factor	**SVF**	Average sky view factor within the grid cell.	$SVF = \frac{1}{n_p} \sum_{j=1}^{n_p} SVF_j$	**3D**

3.4.1 2D INDICATORS

Building Total Area

BTA quantifies the horizontal extent of the built environment within each 1 km tile. The building footprint was derived from the LiDAR classification (class 6 – Buildings), converted into a binary raster, and the total built-up area was obtained by summing all building pixels inside each tile. This indicator reflects surface sealing and the degree of urbanization.

Density of Roads

DR quantifies the intensity of the road network within each tile. Road vectors from OSM (motorway, trunk, primary, secondary, tertiary, residential and service) were clipped to the 1 km grid, and their total length within each tile was measured. The indicator corresponds to the ratio between the summed road length and the tile area, providing a normalized measure of road-network concentration rather than the physical area occupied by roads.

Impervious Surface Ratio

ISR quantifies the intensity of artificial land cover within the parts of each tile corresponding to ground-level LiDAR surfaces. Impervious areas were extracted from class 100 (Artificialized area) of the COS 2024 and intersected with LiDAR classes 1 (Other), 2 (Ground), and 26 (Bridges). The ratio is defined as:

$$ISR = \frac{\text{Impervious area (COS} \cap \text{LiDAR classes 1,2,26)}}{\text{Total area of LiDAR classes 1,2,26}} \quad (3.1)$$

This ensures that artificial surfaces are measured only where the ground is observable in the LiDAR data, while building rooftops are excluded from ISR and represented separately by the building-related indicators

3.4.2 3D INDICATORS

Three-dimensional urban morphology indicators were computed to characterize the vertical structure of the built and vegetated environment, which plays a key role in modulating surface temperature patterns. These indicators were derived from LiDAR data and height-based raster products and capture both the intensity and vertical organization of buildings and vegetation. Figure 6 summarizes the processing workflows used to extract building-related and vegetation-related 3D features, which form the basis for the indicators described below.

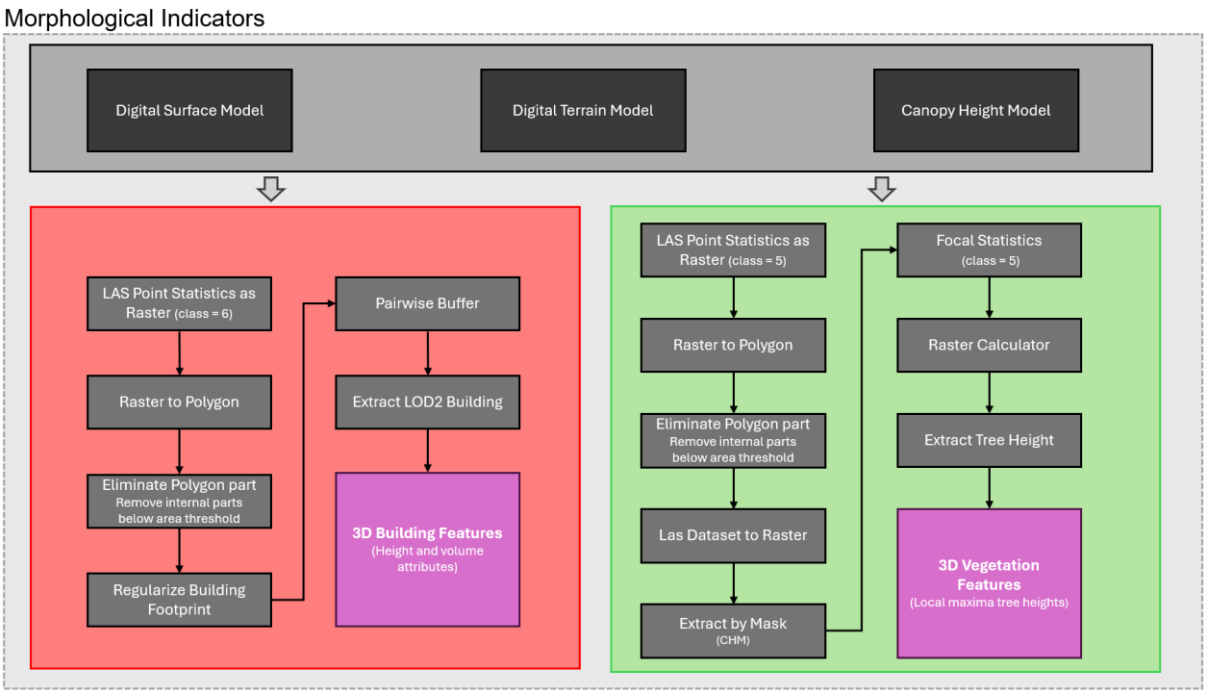

Figure 6 : 3D building feature extraction workflow

BUILDING-RELATED 3D INDICATORS (ABH, ABV, BR)

Building-related 3D indicators were derived from LiDAR-based building features representing the height and volumetric properties of individual structures. These features were obtained by combining Digital Surface Model (DSM) and Digital Terrain Model (DTM) information with LiDAR building classifications, allowing the extraction of building height and volume attributes at the tile level (Figure 4).

- **Average Building Height (ABH) -** represents the mean vertical extent of buildings within each tile and provides a measure of the overall height profile of the built environment.
- **Average Building Volume (ABV) -** quantifies the volumetric intensity of buildings by aggregating height, morphology and footprint information, capturing both horizontal and vertical building density.
- **Building Ratio (BR) -** expresses the proportion of built volume relative to the total tile volume, providing a three-dimensional representation of building compactness.

In this study, BR was computed as the ratio between the number of LiDAR points classified as buildings and the number of LiDAR points classified as ground within each tile, providing a point-density-based proxy for three-dimensional building compactness.

VEGETATION-RELATED 3D INDICATOR (ATH)

Vegetation structure was characterized using a height-based indicator derived from the Canopy Height Model (CHM). Tree height features were extracted by identifying local maxima within vegetated areas, representing dominant tree crowns rather than continuous canopy surfaces (Figure 4).

- **Average Tree Height (ATH) -** corresponds to the mean height of dominant trees within each tile, calculated from local height maxima. This approach captures the vertical influence of urban trees while reducing bias from low or fragmented vegetation.

SKY VIEW FACTOR (SVF)

The SVF was used to describe the degree of sky exposure at ground level, reflecting the combined effect of surrounding buildings and vegetation on radiative exchange. SVF was derived from the Digital Surface Model using the SAGA Next Generation Sky View Factor algorithm implemented in QGIS. The resulting SVF raster represents the fraction of visible sky at each pixel, and tile-level SVF values were obtained by computing the mean SVF within each 1 km tile.

To provide an overview of the spatial distribution of the urban morphology indicators considered in this study, a consistent cartographic layout was adopted for the visualization of all eight variables. Appendix 1 illustrates the spatial patterns of two-dimensional and three-dimensional indicators across the study area, with all variables represented using the same analysis grid and spatial extent, while retaining their original units and metric definitions. This representation allows for visual comparison of spatial patterns and heterogeneity across indicators, without implying direct comparability of absolute values. The maps serve to contextualize the spatial structure of the input variables prior to the quantitative modelling stages.

3.5 Thermal Data Processing

Thermal processing was performed to convert multi-temporal Sentinel-3 SLSTR Land Surface Temperature (LST) acquisitions into robust daytime and nighttime composites. Because individual satellite overpasses may contain residual cloud contamination, data gaps, or short-term variability, a temporal compositing approach was applied. Multiple valid observations were aggregated to generate seasonal daytime and nighttime composites, thereby enhancing data stability and reducing noise. This approach reduces noise and outliers while improving spatial coverage and generating more stable representations of typical summer thermal conditions.

The main steps of the thermal processing workflow are summarized in Figure 7.

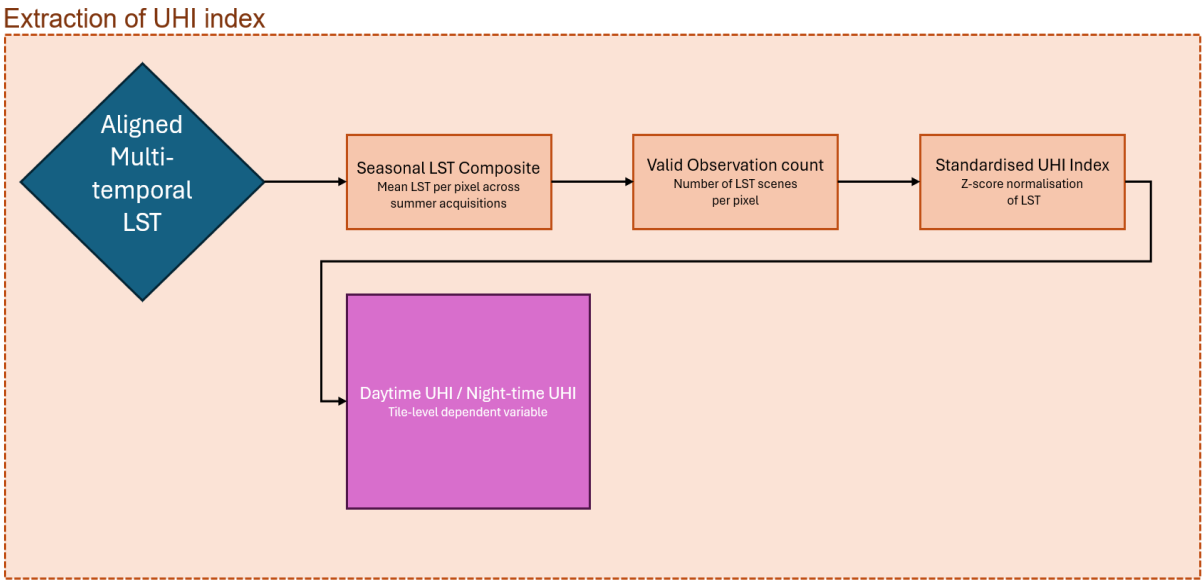

Figure 7 : Thermal data processing workflow

After all daytime and night-time scenes were co-registered to the common analytical grid (Section 3.2), two seasonal composites were produced: one representing daytime conditions and one representing night-time conditions. For each period, the pixel-level mean LST was computed from the available summer acquisitions (approximately 14 images per period) using the GRASS GIS r.series tool within QGIS.

In parallel, a second set of composites was generated using the count statistic, recording the number of valid observations contributing to each pixel of the mean composite. These layers served as a quality-control output, allowing the identification of areas where the mean temperature was derived from fewer valid observations.

To derive the Urban Heat Island index, the mean daytime and night-time LST composites were transformed into standardized temperature anomalies using a z-score formulation:

$$UHI = \frac{T_i - \bar{T}}{\sigma} \quad (3.2)$$

T_i - composite LST value at pixel i

$\bar{T}$ - mean LST across the study area

σ - standard deviation of LST

This transformation yields a dimensionless index indicating the relative thermal deviation of each pixel from the overall municipal temperature distribution, with positive values representing warmer conditions and negative values indicating cooler conditions. The procedure was conducted separately for daytime and night-time composites, producing two distinct UHI rasters that capture diurnal and nocturnal heat patterns during the summer period. Subsequently, UHI values were aggregated to the 1 km analytical grid using zonal statistics, generating a single representative UHI value per tile to be used as the dependent variable in the subsequent modelling stage.

3.6 MODELING FRAMEWORK

The modelling framework is based on the Light Gradient Boosting Machine (LightGBM), a tree-based ensemble learning algorithm that builds an additive model through gradient boosting of decision trees (Ke et al., 2017; Han et al., 2025). LightGBM has been increasingly adopted in urban climate and remote sensing studies due to its ability to model complex, nonlinear relationships between heterogeneous predictors while remaining computationally efficient (Zhou et al., 2016).

In the context of urban thermal environments, relationships between morphological indicators and UHI intensity are rarely linear and often exhibit threshold effects and interactions between variables such as urban geometry, surface sealing, and vegetation structure (Oke et al., 2017) .Tree-based ensemble models are well suited to capture these behaviors without requiring explicit specification of interaction terms. LightGBM was therefore selected as a flexible, non-parametric modelling approach capable of accommodating the complexity of urban thermal processes.

The choice of LightGBM was independent of dataset size. The limited number of spatial units is treated as a study constraint, and model configuration and validation were defined accordingly to reduce overfitting and preserve interpretability

3.6.1 DATABASE CONSTRUCTION

The final modelling dataset was structured as a tabular matrix in which each row corresponds to a grid tile and each column represents either the target thermal variable or a morphological predictor. This format facilitates reproducibility and direct integration with machine learning workflows. Prior to model training, the dataset was screened for missing and non-finite values, which were removed to ensure numerical stability. No scaling or normalization of predictor variables was applied, as tree-based models such as LightGBM are invariant to monotonic transformations of the input features. This choice preserves the original physical meaning of the morphological indicators and avoids unnecessary preprocessing steps. Extreme UHI values were retained when they corresponded to physically meaningful urban configurations, such as large urban parks, in order to preserve the diversity of thermal regimes present in the study area. This decision reflects the explanatory focus of the modelling framework, which aims to capture real urban contrasts rather than optimize predictive accuracy.

3.6.2 LIGHTGBM MODELLING AND VALIDATION

Model hyperparameters were defined to prioritize generalization and interpretability rather than maximizing predictive accuracy. Model complexity, learning dynamics, regularization and subsampling strategies were deliberately constrained to promote stable learning and reduce sensitivity to individual spatial units. The main configuration choices and their methodological rationale are summarized in Table 4.

Given the limited number of analytical units and the explanatory focus of the study, extensive hyperparameter optimization procedures such as grid search or Bayesian optimization were intentionally avoided, as they may lead to unstable solutions and overfitting in small datasets (Hawkins, 2003). Instead, parameter values were selected based on methodological recommendations and exploratory testing to ensure reproducible and interpretable model behavior.

Model performance was evaluated using five-fold cross-validation as a diagnostic of robustness rather than predictive skill (James et al., 2021).

The coefficient of determination (R^2) and the root mean square error (RMSE) were used to contextualize model behavior, with R^2 indicating the proportion of variance explained and RMSE expressing the average error in physical units (°C), which is particularly relevant in urban climate analyses (Stewart & Oke, 2012). Predictor variables were retained in their original scale, consistent with the properties of tree-based models, and to preserve the physical interpretability of feature contributions during the explainability stage.

Table 4: LightGBM hyperparameter configuration and modelling rationale

Model aspect	Hyperparameters involved	Configuration rationale
Model complexity	Tree depth, number of leaves	Constrained to limit model flexibility and reduce overfitting in a small-sample setting
Learning dynamics	Learning rate, number of estimators	Configured to favor gradual learning and stable convergence rather than rapid optimization
Node splitting	Minimum samples per leaf	Restricted to prevent overly specific splits driven by individual tiles
Observation subsampling	Subsample ratio	Enabled to increase robustness and reduce sensitivity to individual observations
Feature subsampling	Feature sampling ratio	Enabled to limit feature dominance and improve generalization
Regularization	L1 and L2 penalties	Applied to penalize complex models and stabilize parameter estimates

3.6.3 MODEL INTERPRETABILITY USING SHAP

Model interpretability is a central requirement of this study, as the objective is to understand how urban morphological characteristics contribute to spatial variations in UHI intensity rather than to produce purely predictive outputs. In an urban planning and climate adaptation context, interpretable models are essential for translating data-driven results into physically meaningful insights that can inform design and policy decisions. Accordingly, the modelling framework prioritizes transparency in the relationship between input variables and model outputs. To interpret the LightGBM model, SHapley Additive exPlanations (SHAP) were employed as a post-hoc interpretability framework, meaning that explanations are derived after model training without influencing the model itself. SHAP is grounded in cooperative game theory and provides an additive decomposition of each model prediction into feature-specific contributions, allowing both the magnitude and direction of influence to be quantified (Lundberg & Lee, 2017). Positive SHAP values indicate an increase in UHI intensity relative to the model baseline, while negative values indicate a cooling effect, enabling direct comparison across variables with different units and distributions. Model behavior was analyzed at both global and local scales: global explanations, based on

mean absolute SHAP values, identify the most influential morphological drivers of UHI variability across the study area, whereas local explanations and dependence plots reveal non-linear responses and context-dependent effects associated with specific urban configurations. Although SHAP provides a robust and transparent interpretative framework, SHAP values describe associations learned by the model rather than causal relationships. Results should therefore be interpreted as indicative patterns, conditioned by the available data and model configuration, rather than as universal or deterministic rules.

4. RESULTS AND DISCUSSION

This chapter presents and discusses the results obtained from the analysis of the Urban Heat Island (UHI) phenomenon and its relationship with urban morphological characteristics within the study area. The analyses are designed to address the core research questions of this thesis, namely how the spatial patterns of UHI intensity vary between daytime and nighttime conditions, and to what extent two-dimensional and three-dimensional urban morphology indicators contribute to explaining this variability. The chapter is structured to progressively move from a descriptive assessment of observed thermal data patterns to a data-driven interpretation of their underlying drivers. First, the spatial distribution of the standardized UHI index is examined for both daytime and nighttime conditions, highlighting major spatial gradients, diurnal contrasts, and persistent thermal anomalies across the city. This initial assessment establishes the empirical context for the modelling stage. Subsequently, the performance of the LightGBM models is evaluated, followed by an interpretation of the relative importance and behaviour of urban morphology indicators using SHAP-based explainable machine learning techniques. These analyses allow a detailed examination of how different aspects of urban form influence UHI intensity under contrasting thermal regimes.

By integrating spatial analysis, predictive modelling, and model interpretability, this chapter links the research questions posed in the introductory chapters with quantitative results and physically meaningful interpretations.

4.1 Spatial Patterns of the Urban Heat Island Index

The UHI index used in the following figures (8 & 9) analyses corresponds to the standardized LST anomalies derived from the seasonal daytime and nighttime composites, as described in the methodological section. After transformation, values were spatially aggregated to the 1 km analytical grid to ensure consistency with the urban morphology indicators and to define the dependent variable for subsequent modelling. This aggregation step produces a single representative UHI value per grid cell, enabling direct comparison between thermal patterns and structural characteristics of the built environment.

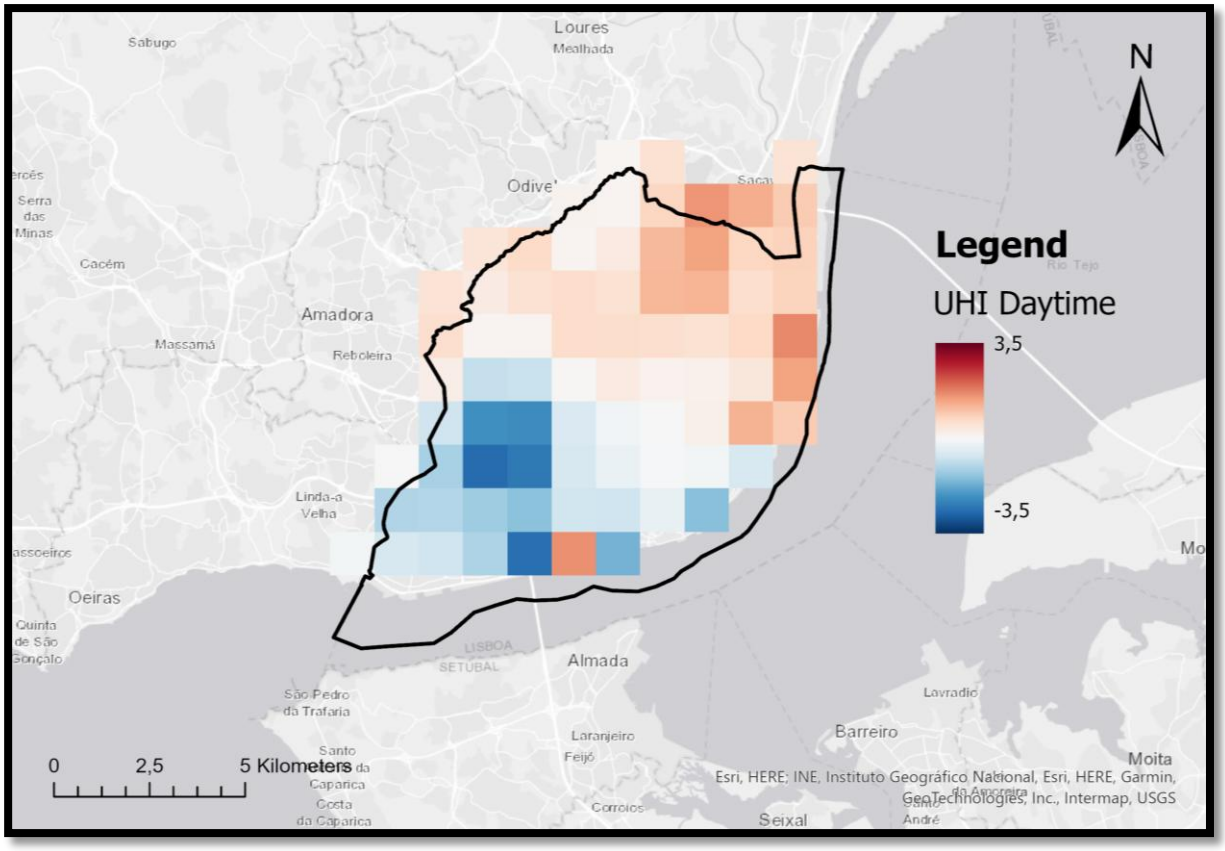

Figure 8 : Standardized daytime UHI map

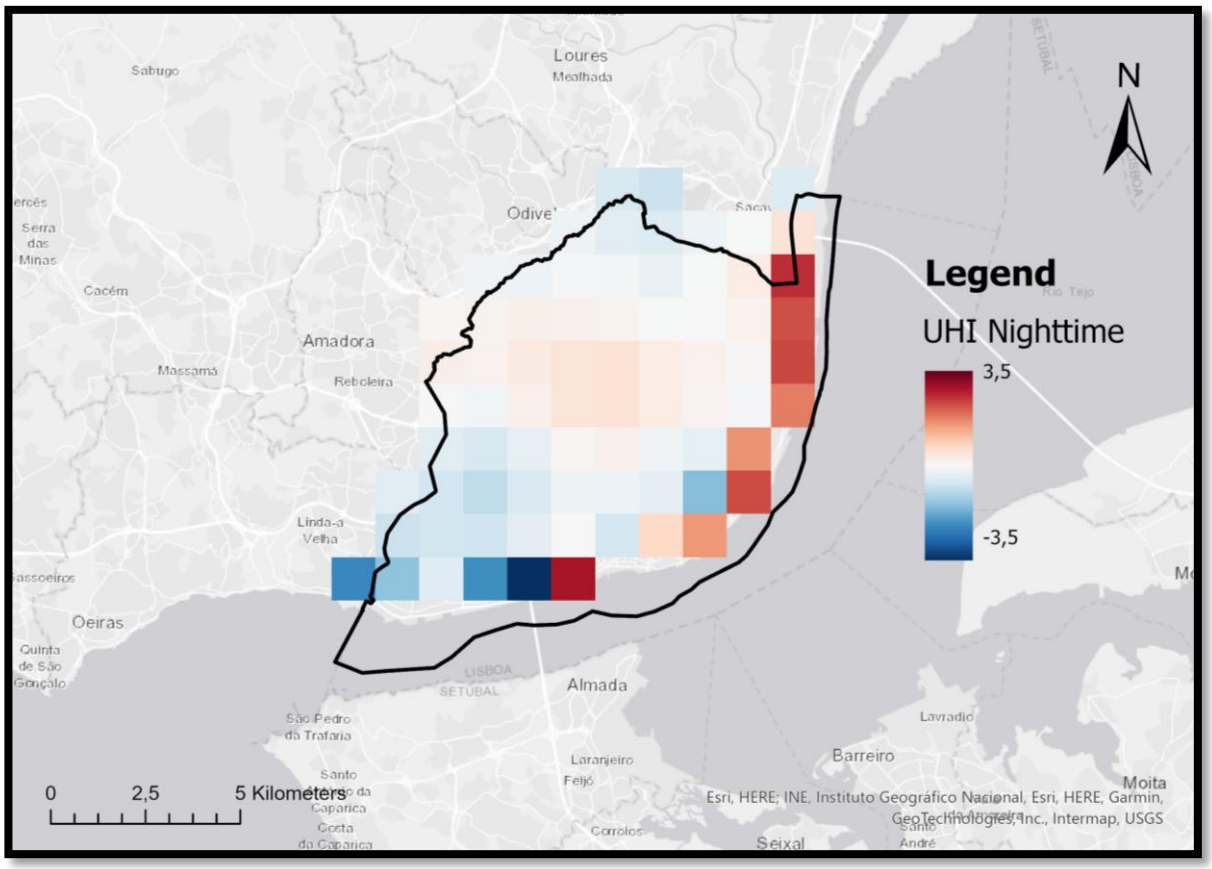

Figure 9 : Standardized nighttime UHI map

During daytime conditions, the UHI pattern exhibits a clear spatial gradient across the municipality. Higher positive UHI values are predominantly observed in the northern and northeastern sectors of the city, which include the airport area and surrounding zones characterized by transport infrastructure, industrial land use, and a high proportion of impervious surfaces. These areas are associated with extensive paved surfaces and limited vegetation cover, favoring increased surface heating during daytime hours. In contrast, negative UHI values, indicating relatively cooler surface conditions, are concentrated in the southwestern portion of the study area, particularly in areas dominated by large contiguous green spaces such as the Monsanto green corridor. The presence of dense tree cover and lower building density in this sector promotes shading and evapotranspiration, contributing to reduced daytime surface temperatures relative to more urbanized areas. The nighttime UHI pattern reveals persistent positive anomalies in the eastern sector of the municipality, particularly along the riverfront areas. Contrary to what might be expected from the presence of a large water body, the spatial distribution does not indicate a systematic nocturnal cooling effect associated with proximity to the Tagus estuary. Similar spatial configurations have been previously documented for Lisbon, where nocturnal UHI intensity was found to be strongly influenced by urban structure and surface thermal properties rather than mesoscale cooling mechanism (Oliveira et al., 2021).

4.2 Performance of the LightGBM Models

The performance of the LightGBM models was evaluated using a 5-fold cross-validation framework, with accuracy assessed through the coefficient of determination (R^2) and the root mean square error (RMSE) for both daytime and nighttime conditions. This approach ensures that model behavior remains stable across different data partitions, providing a consistent basis for interpretation. While R^2 indicates the proportion of spatial variability in UHI intensity captured by the model, RMSE reflects the average magnitude of residual error. This evaluation was conducted to confirm the robustness of the modelling framework prior to analyzing the contribution of individual predictors. The outcomes of this validation procedure are presented in Table 5, which synthesizes the model performance across the cross-validation folds for both daytime and nighttime conditions.

Table 5 : Cross-validation performance metrics

Model	R^2 (mean)	RMSE (mean)
Daytime UHI	0.306	0.783
Nighttime UHI	0.198	0.302

For daytime conditions, the model achieved an average R^2 of 0.306 and an RMSE of 0.783, with consistently positive R^2 values across all folds. This indicates a stable ability to capture a meaningful proportion of the spatial variability in daytime UHI intensity, despite the large amplitude of daytime surface temperature contrasts driven by radiative processes and surface heterogeneity.

The nighttime model yielded a lower average R^2 of 0.198 and an RMSE of 0.302, with greater variability between folds, including one negative R^2 value. This reduced and less stable performance reflects the increased complexity of nocturnal thermal processes, where heat storage, delayed release from urban materials, and atmospheric stability play a dominant role. Given the relatively limited sample size and the use of static morphological predictors, such performance differences between daytime and nighttime conditions are consistent with expectations.

Reduced-variable model configurations were explicitly tested but did not result in improved predictive performance. Consequently, the full set of urban morphology indicators was retained for the main analysis, while reduced-variable configurations were used exclusively for sensitivity testing. The following section therefore focuses on interpreting the contribution of individual indicators using SHAP-based explainable machine learning techniques.

4.3 Global Importance of Urban Morphology Indicators

The SHAP summary plots provide an overview of the global importance of urban morphology indicators under daytime and nighttime conditions. As illustrated in Figures 10 and 11, the horizontal axis represents the SHAP value, indicating the direction and strength of each variable's contribution to predicted UHI intensity (positive values increasing UHI and negative values decreasing it), while the color scale reflects the

magnitude of the feature values. These plots highlight not only the most influential predictors but also the variability and context-dependent nature of Urban Heat Island processes.

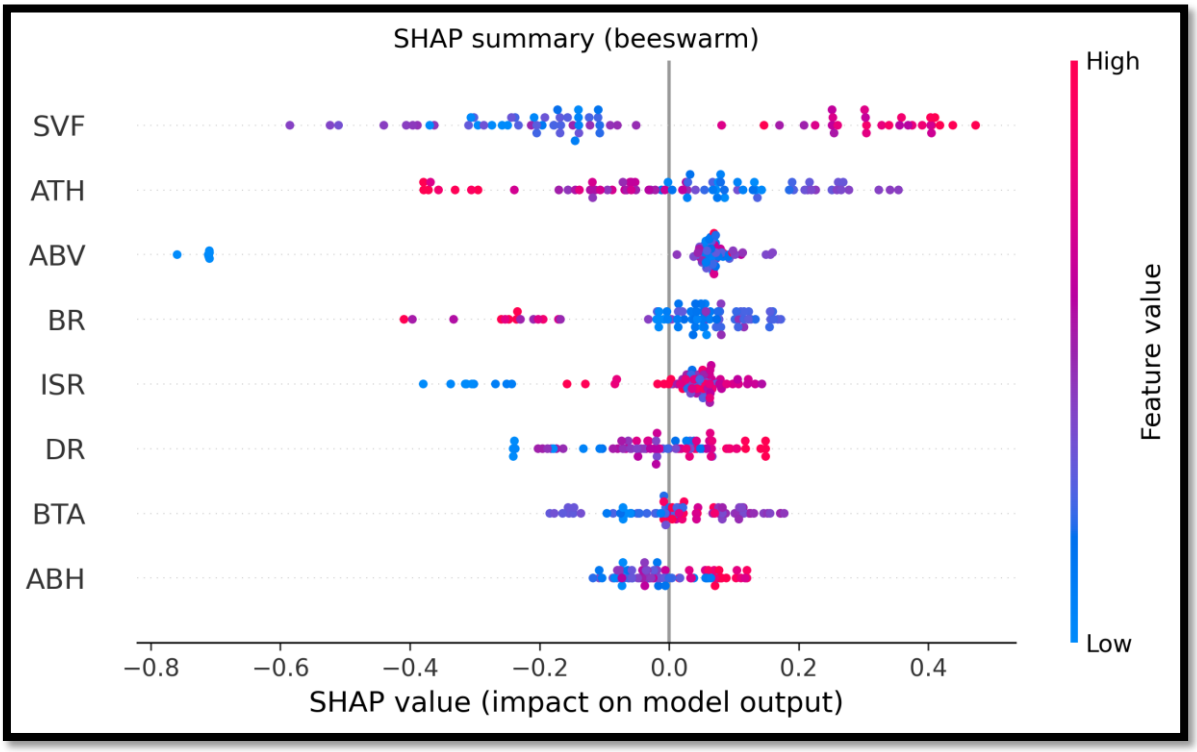

Figure 10 : SHAP summary (beeswarm) plot for daytime

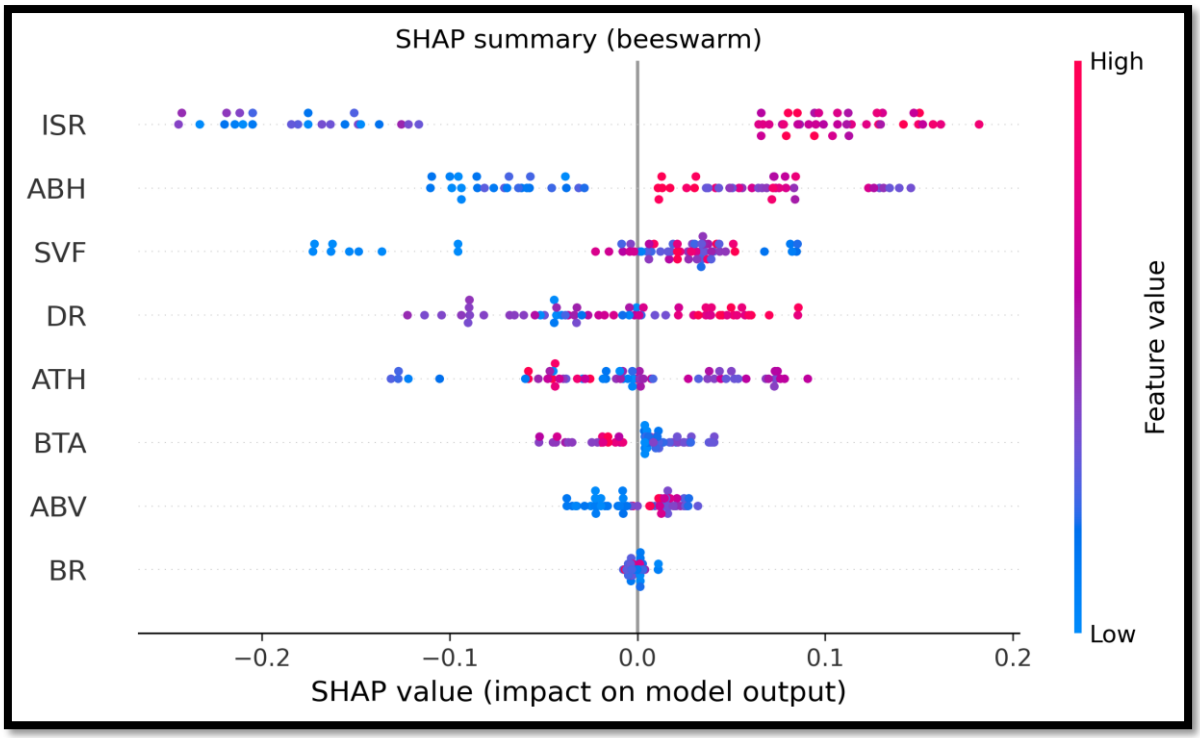

Figure 11 : SHAP summary (beeswarm) plot for nighttime

During daytime conditions, the beeswarm plot indicates that Sky View Factor (SVF) and average tree height (ATH) exhibit broad distributions of SHAP values, reflecting substantial spatial variability in their influence on UHI intensity. In contrast, average building volume (ABV), while still ranking among the most influential indicators, shows a comparatively more concentrated distribution of positive SHAP values, suggesting a more consistent effect across the study area. The wide spread of SHAP values associated with these indicators suggests that their effects are highly context-dependent and vary across different urban configurations. Higher SVF values are associated with positive SHAP values, indicating increased daytime UHI in more open urban environments, likely due to enhanced solar exposure and reduced shading. In contrast, lower SVF values contribute negatively to the model output, consistent with shading effects in more enclosed urban canyons.

Average Tree height indicator displays mixed but structured SHAP patterns, with both positive and negative contributions depending on their magnitude and spatial context. This behavior highlights the non-linear nature of vegetation effects on daytime surface temperatures, where cooling benefits from shading and evapotranspiration may be modulated by surrounding built form, surface materials, and exposure conditions. The pronounced dispersion observed for these variables indicates that daytime UHI processes are governed by a combination of interacting factors rather than by a single dominant mechanism.

At night, the beeswarm plot reveals a marked shift in both the distribution and dominance of feature effects. Impervious surface ratio (ISR) and average building height (ABH) show consistently positive SHAP values at higher feature levels, with comparatively narrower spreads than those observed during daytime conditions. This reduced dispersion suggests a more systematic and uniform relationship between dense, vertically developed urban areas and elevated nighttime UHI intensity. In contrast to daytime patterns, indicators related to vegetation and sky openness exhibit lower SHAP magnitudes and more clustered distributions, implying a diminished and more homogeneous influence under nocturnal conditions.

Table 6 summarizes the relative contribution of each urban morphology indicator to the LightGBM model predictions for daytime and nighttime conditions, providing a concise synthesis of variable dominance across day-night regimes

Table 6 : Importance of urban morphology indicators in the model

Indicator	Daytime importance (%)	Nighttime importance (%)	General influence pattern
SVF	28.6	12.2	Generally, increases UHI under higher openness
ATH	15.8	11.4	Context-dependent cooling, modulated by surrounding morphology
ABV	13.1	4.5	Generally associated with higher UHI
BR	11.1	0.8	Tends to reduce UHI, particularly at higher values
ISR	9.2	35.9	Strong and consistent increase in UHI
DR	8.5	12.0	Generally associated with higher UHI
BTA	7.8	5.0	Weak to moderate cooling effect
ABH	5.9	18.1	Consistently increases UHI, especially at night

The ranking confirms the predominance of openness- and vegetation-related indicators during daytime conditions, with Sky View Factor and vegetation metrics occupying the top positions. In contrast, nighttime conditions are characterized by a clear shift towards built-environment indicators, particularly impervious surface ratio and average building height, which together account for a substantial proportion of the

total model importance. This reordering of dominant predictors reflects a transition from highly heterogeneous, radiatively driven processes during the day to more uniform mechanisms governed by heat storage and urban geometry at night, reinforcing the importance of explicitly accounting for diurnal dynamics when interpreting the influence of urban morphology on UHI intensity.

4.4 Non-linear and Context-Dependent Effects

While global feature importance provides an overview of the dominant drivers of UHI variability, it does not capture how the influence of individual urban morphology indicators changes across different value ranges or urban contexts. To address this limitation, SHAP dependence plots were analyzed for a selected set of indicators. These plots explicitly depict the relationship between each indicator and its contribution to UHI intensity, allowing non-linear responses, threshold effects, and interaction-driven variability to be examined.

The dependence plots were generated separately for daytime (Figure 12) and night-time (Figure 13) conditions using the same subset of indicators, enabling a direct comparison of diurnal differences in the functional relationships between urban form and thermal response. This comparative perspective is particularly relevant in urban climate studies, as the physical mechanisms governing UHI dynamics differ markedly between day and night, shifting from radiative and surface–atmosphere interactions to processes dominated by heat storage and release.

By focusing on indicator-specific response patterns rather than average effects, this analysis highlights the contextual nature of urban thermal behavior and provides insights into how morphological characteristics may contribute differently to UHI intensity depending on both their magnitude and the time of day.

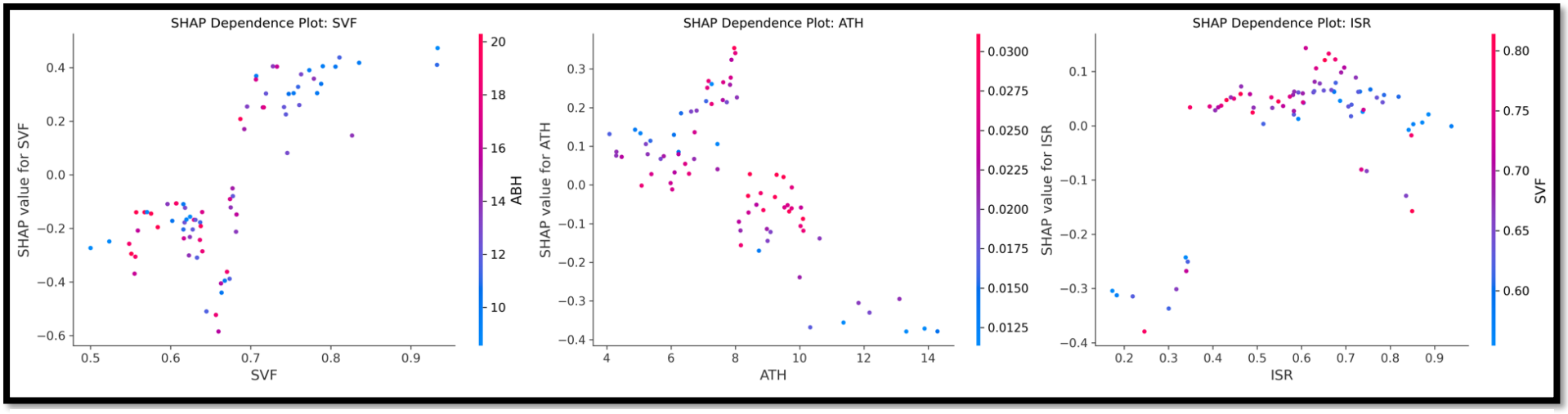

Figure 12 : SHAP dependence plots for selected morphological indicators on daytime conditions

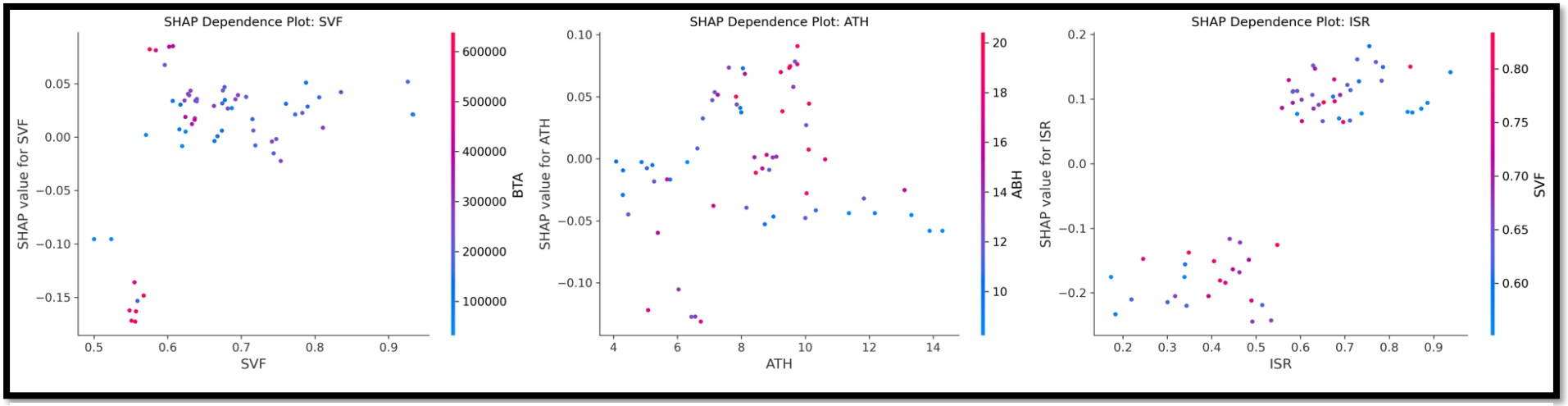

Figure 13: SHAP dependence plots for selected morphological indicators on nighttime conditions

The SHAP dependence plots reveal that the influence of urban morphology indicators on UHI intensity is strongly non-linear and varies substantially between daytime and nighttime conditions. During the day (Figure 12), the relationships are characterized by high dispersion and pronounced context dependency, reflecting the dominance of radiative processes and surface–atmosphere interactions. Indicators related to urban openness, vegetation structure, and surface sealing exhibit non-linear responses, whereby their contribution to UHI intensification or mitigation varies across value ranges and local configurations. In general, more open urban forms tend to enhance daytime UHI through increased solar exposure, while vegetation-related characteristics contribute to cooling effects that become progressively weaker at higher values.

In contrast, nighttime conditions are marked by more systematic and less dispersed functional relationships (Figure 13). The dependence plots indicate that UHI intensity is primarily governed by impervious surfaces and built geometry, with higher values consistently associated with increased nocturnal warming. This reduced variability points to the dominant role of heat storage and delayed heat release from urban materials, while the influence of vegetation and sky openness becomes secondary once radiative cooling and evapotranspiration are suppressed.

Across both diurnal regimes, the dependence plots further suggest the presence of threshold and saturation effects for selected indicators. For Sky View Factor during daytime conditions, UHI intensification becomes more pronounced beyond intermediate values (approximately SVF ≈ 0.65–0.7), indicating that increased openness only translates into substantial warming once a minimum level of solar exposure is reached. A comparable pattern is observed for impervious surface ratio under nighttime conditions, where UHI contributions become consistently positive beyond intermediate values (approximately ISR ≈ 0.5), indicating that once a substantial proportion of surface sealing is reached, additional imperviousness is systematically associated with increased nocturnal warming. Vegetation-related indicators display more gradual and context-dependent responses, with cooling effects gradually strengthening as vegetation height increases, although the magnitude of this effect varies depending on surrounding urban structure.

Overall, the contrast between daytime and nighttime dependence patterns highlights a shift from heterogeneous, surface-driven mechanisms to more uniform processes governed by urban structure and thermal inertia

4.5 Implications of the Results for Understanding Urban Heat Island Processes

The results presented in the previous sections can be interpreted coherently within the framework of established Urban Heat Island (UHI) theory. Rather than simply reflecting differences between daytime and nighttime conditions, the observed diurnal contrasts illustrate how the explanatory relevance of morphology-based indicators depends on the dominant physical processes governing urban thermal behavior. Adopting a diurnal perspective therefore provides a structured basis for interpreting when and how two-dimensional and three-dimensional urban morphology descriptors meaningfully contribute to UHI variability.

These findings directly address the research questions guiding this thesis. First, the results confirm that spatial patterns of UHI intensity in Lisbon differ substantially between daytime and nighttime conditions, not only in magnitude but also in structural organization. Second, the modelling framework demonstrates that both two-dimensional and three-dimensional morphology indicators contribute to explaining this variability; however, their explanatory relevance is temporally conditioned, varying across the diurnal cycle.

From a theoretical standpoint, the results align with classical urban climate formulations that distinguish between radiatively driven surface processes during daytime and storage-dominated mechanisms during nighttime (Oke, 2002; Stewart & Oke, 2012). The modelling outcomes indicate that urban morphology contributes to observed UHI patterns under both diurnal regimes; however, its explanatory capacity varies across the diurnal cycle. During daytime conditions, UHI variability emerges from complex and highly interactive processes involving solar exposure, shading, vegetation, and surface characteristics. These interactions lead to pronounced spatial heterogeneity and non-linear responses, such that static morphological indicators are able to capture relative spatial patterns but cannot fully resolve the variability introduced by transient radiative and atmospheric processes.

In contrast, nighttime conditions are characterized by more stable and systematic relationships between urban form and thermal behavior, reflecting the dominance of heat storage, delayed release, and geometric confinement. Under these conditions, indicators describing imperviousness and three-dimensional built structure exhibit more internally consistent relationships with nocturnal UHI intensity, in line with previous studies emphasizing the role of urban geometry and volumetric properties in shaping nighttime thermal patterns (S. Grimmond, 2007).In the specific context of Lisbon, these findings are consistent with previous LCZ-based analyses showing elevated thermal intensities in compact and highly impervious urban classes (Matias & Lopes, 2024). The present study extends these observations by quantifying the relative contribution of three-dimensional morphological structure within an interpretable modelling framework, thereby refining the understanding of how volumetric properties influence nocturnal heat retention in the city.

More broadly, the identification of non-linear responses and threshold behavior across multiple indicators reinforces recent research demonstrating that the influence of urban morphology on temperature does not scale linearly with changes in form or land cover (Zhang et al., 2025). Instead, morphological indicators exert a conditional influence, becoming thermally relevant only beyond specific configurations or value ranges. The use of explainable machine learning techniques enables these dynamics to be explicitly identified, while clarifying the contexts in which morphology-based descriptors are most and least effective.

From a planning perspective, these results highlight the importance of integrating three-dimensional urban structure into heat mitigation strategies. While vegetation and surface-based interventions remain central for reducing daytime heat exposure, the stronger and more systematic relationship between built form and nocturnal UHI intensity suggests that volumetric density, canyon geometry, and impervious surface concentration play a critical role in nighttime heat retention. Incorporating such morphological considerations into urban redevelopment, densification, and climate adaptation policies may enhance the effectiveness of heat mitigation strategies in Mediterranean cities such as Lisbon.

Nevertheless, the explanatory capacity of morphology-based indicators remains constrained by the spatial resolution of the thermal data and by the inherently dynamic nature of urban–atmosphere interactions. Static structural descriptors cannot fully capture short-term meteorological variability, particularly under daytime radiative

forcing. These limitations partially explain the lower explanatory strength observed in the daytime models and underscore the need for integrating structural metrics with high-resolution atmospheric observations in future research.

More broadly, as climate change intensifies the frequency and severity of heat extremes, understanding how urban structure conditions thermal exposure becomes increasingly critical. Future research may benefit from integrating dynamic land–atmosphere modelling, temporally adaptive morphological indicators, and cross-city comparative analyses to further disentangle structural and atmospheric contributions to UHI variability. Expanding such integrated frameworks across Mediterranean urban contexts would strengthen comparative understanding and support evidence-based climate adaptation planning.

Taken together, this interpretative synthesis situates the empirical findings within established UHI theory, responds directly to the research questions of the study, and clarifies the conditions under which two-dimensional and three-dimensional urban morphology indicators provide meaningful explanatory insight. At the same time, it delineates the methodological and contextual boundaries of their applicability, offering a foundation for continued refinement of integrated urban climate analysis.

6. CONCLUSIONS AND FUTURE RESEARCH

This study set out to examine the extent to which two-dimensional and three-dimensional urban morphology indicators can explain the spatial variability of Urban Heat Island intensity under daytime and nighttime conditions. The results show that morphology-based descriptors can capture meaningful spatial patterns in UHI intensity, particularly when diurnal dynamics are explicitly considered and three-dimensional structure is incorporated. At the same time, the findings indicate that while urban morphology provides a coherent framework for interpreting UHI variability, it does not offer a complete representation of urban thermal behavior, which is shaped by multiple interacting processes that vary over the full diurnal cycle.

Taken as a whole, the results reveal that the capacity of urban morphology indicators to explain UHI variability is not uniform, but strongly dependent on the temporal context in which thermal patterns emerge. The analyses show that morphology-based descriptors are particularly effective at capturing spatial regularities associated with persistent structural characteristics of the urban environment, while their explanatory relevance diminishes where temperature variability is dominated by highly transient and locally contingent processes. This distinction becomes evident when contrasting diurnal conditions, where spatial patterns are more heterogeneous and context-specific, with periods in which thermal behavior is more closely linked to the enduring physical configuration of the city. Viewed in this way, urban morphology emerges not as a universal predictor of UHI intensity, but as a conditional explanatory framework whose relevance depends on the interaction between urban form, time, and dominant thermal processes. This conditionality reflects the fact that urban heat dynamics arise from coupled surface–atmosphere processes that extend beyond morphology alone.

Despite the insights provided by this analysis, several limitations should be acknowledged. A primary constraint relates to the spatial resolution of the satellite-derived land surface temperature data, which, while appropriate for capturing mesoscale urban thermal patterns, limits the representation of fine-scale intra-urban variability. As a result, localized thermal contrasts associated with individual streets, parcels, or microclimatic features cannot be fully resolved. Established approaches combining satellite-derived surface temperatures with ground-based sensor networks have been shown to support cross-validation and enhance the interpretation of local

thermal conditions. Although this integration was outside the scope of the present study, it represents a natural extension for future analyses.

The analysis is also constrained by data availability, both in terms of ancillary environmental variables and temporal coverage. Although the inclusion of additional datasets, such as atmospheric measurements, surface material properties, or human activity indicators could further refine the interpretation of UHI processes, this study prioritized methodological consistency by maintaining methodological continuity with existing studies, thereby allowing the results to be interpreted within a broader and comparable research context.

Similarly, urban morphology indicators derived from LiDAR and remote sensing represent abstractions of complex urban structures and were not subject to direct field-based validation although, careful preprocessing, sensitivity testing, and internal consistency checks were undertaken throughout the analysis to minimize potential uncertainties. These considerations highlight that the results should be interpreted as structurally informed representations of urban form rather than exact physical measurements, while also pointing to clear opportunities for future validation and methodological refinement. Building on these considerations, future research should focus on extending morphology-based UHI analyses through the integration of complementary data sources and modelling strategies. In particular, combining satellite-derived surface temperatures with dense networks of ground-based sensors would allow more robust validation of remotely sensed thermal patterns and improve the representation of local-scale variability. Further advances could also be achieved by incorporating additional atmospheric and surface-related variables, as well as by expanding the temporal scope of analysis to capture seasonal and interannual dynamics.

From a methodological perspective, continued development of explainable machine learning frameworks offers promising opportunities to better integrate three-dimensional urban morphology with dynamic processes, helping to clarify the conditions under which urban form exerts a dominant influence on thermal behavior. Together, these directions point toward a more integrated and process-aware approach to urban climate analysis, in which morphology remains a key structural component while being interpreted within a broader environmental and temporal context.

BIBLIOGRAPHICAL REFERENCES

Afroosheh, S., & Askari, M. (2024). *Fusion of Deep Learning and GIS for Advanced Remote Sensing Image Analysis*. https://arxiv.org/pdf/2412.19856

Arnfield, A. J. (2003). Two decades of urban climate research: A review of turbulence, exchanges of energy and water, and the urban heat island. *International Journal of Climatology*, *23*(1), 1–26. https://doi.org/10.1002/joc.859

Bechtel, B., See, L., Mills, G., & Foley, M. (2016). Classification of Local Climate Zones Using SAR and Multispectral Data in an Arid Environment. *IEEE Journal of Selected Topics in Applied Earth Observations and Remote Sensing*, *9*(7), 3097–3105. https://doi.org/10.1109/JSTARS.2016.2531420

Chajaei, F., & Bagheri, H. (2024a). Machine learning framework for high-resolution air temperature downscaling using LiDAR-derived urban morphological features. *Urban Climate*, *57*. https://doi.org/10.1016/J.UCLIM.2024.102102

Chajaei, F., & Bagheri, H. (2024b). Machine learning framework for high-resolution air temperature downscaling using LiDAR-derived urban morphological features. *Urban Climate*, *57*, 102102. https://doi.org/10.1016/J.UCLIM.2024.102102

Chajaei, F., & Bagheri, H. (2024c). Machine learning framework for high-resolution air temperature downscaling using LiDAR-derived urban morphological features. *Urban Climate*, *57*, 102102. https://doi.org/10.1016/J.UCLIM.2024.102102

Chakraborty, T., & Lee, X. (2019). A simplified urban-extent algorithm to characterize surface urban heat islands on a global scale and examine vegetation control on their spatiotemporal variability. *International Journal of Applied Earth Observation and Geoinformation*, *74*, 269–280. https://doi.org/10.1016/J.JAG.2018.09.015

Deilami, K., Kamruzzaman, M., & Liu, Y. (2018). Urban heat island effect: A systematic review of spatio-temporal factors, data, methods, and mitigation measures. *International Journal of Applied Earth Observation and Geoinformation*, *67*, 30–42. https://doi.org/10.1016/J.JAG.2017.12.009

Estoque, R. C., Murayama, Y., & Myint, S. W. (2017a). Effects of landscape composition and pattern on land surface temperature: An urban heat island study in the megacities of Southeast Asia. *Science of the Total Environment*, *577*, 349–359. https://doi.org/10.1016/J.SCITOTENV.2016.10.195

Estoque, R. C., Murayama, Y., & Myint, S. W. (2017b). Effects of landscape composition and pattern on land surface temperature: An urban heat island study in the megacities of Southeast Asia. *Science of the Total Environment*, *577*, 349–359. https://doi.org/10.1016/J.SCITOTENV.2016.10.195

Foissard, X., Rome, S., Bigot, S., Rousset, E., & Fouvet, A. C. (2024). A new high spatial density temperature dataset in the Grenoble alpine valley (France) for urban heat island investigation and climate services dedicated to municipalities purposes. *Data in Brief*, *55*. https://doi.org/10.1016/J.DIB.2024.110553

Gaur, A., & Deb, C. (2024). *A Review on Machine Learning Approaches for Assessing Urban Heat Islands*. https://doi.org/10.2139/SSRN.4891060

Grimmond, C. S. B., Oke, T. R., Grimmond, C. S. B., & Oke, T. R. (1999). Aerodynamic Properties of Urban Areas Derived from Analysis of Surface Form. *JApMe*, *38*(9), 1262–1292. https://doi.org/10.1175/1520-0450(1999)038

Grimmond, S. (2007). Urbanization and global environmental change: Local effects of urban warming. *Geographical Journal*, *173*(1), 83–88. https://doi.org/10.1111/J.1475-4959.2007.232_3.X;ISSUE:ISSUE:DOI

Han, T., Du, C., Xie, Y., Xian, X., Zhang, X., Yang, B., & Chen, Y. (2025a). A 3D perspective for understanding the mechanisms of urban heat island and urban morphology using multi-modal geospatial data and interpretable machine learning. *Building and Environment*, *282*. https://doi.org/10.1016/J.BUILDENV.2025.113184

Han, T., Du, C., Xie, Y., Xian, X., Zhang, X., Yang, B., & Chen, Y. (2025b). A 3D perspective for understanding the mechanisms of urban heat island and urban morphology using multi-modal geospatial data and interpretable machine learning. *Building and Environment*, *282*, 113184. https://doi.org/10.1016/J.BUILDENV.2025.113184

Hawkins, D. M. (2003). The Problem of Overfitting. *Journal of Chemical Information and Computer Sciences*, *44*(1), 1–12. https://doi.org/10.1021/CI0342472

Imhoff, M. L., Zhang, P., Wolfe, R. E., & Bounoua, L. (2010). Remote sensing of the urban heat island effect across biomes in the continental USA. *Remote Sensing of Environment*, *114*(3), 504–513. https://doi.org/10.1016/J.RSE.2009.10.008

(IPCC), I. P. on C. C. (2023). Climate Change 2021 – The Physical Science Basis: Working Group I Contribution to the Sixth Assessment Report of the Intergovernmental Panel on Climate Change. *Climate Change 2021 – The Physical Science Basis*. https://doi.org/10.1017/9781009157896

James, G., Witten, D., Hastie, T., & Tibshirani, R. (2021). *An Introduction to Statistical Learning*. *Springer Texts in Statistics*. https://doi.org/10.1007/978-1-0716-1418-1

Johansson, E. (2006). Influence of urban geometry on outdoor thermal comfort in a hot dry climate: A study in Fez, Morocco. *Building and Environment*, *41*(10), 1326–1338. https://doi.org/10.1016/J.BUILDENV.2005.05.022

Johansson, E., & Emmanuel, R. (2006). The influence of urban design on outdoor thermal comfort in the hot, humid city of Colombo, Sri Lanka. *International Journal of Biometeorology*, *51*(2), 119–133. https://doi.org/10.1007/S00484-006-0047-6

Ke, G., Meng, Q., Finley, T., Wang, T., Chen, W., Ma, W., Ye, Q., & Liu, T.-Y. (n.d.). *LightGBM: A Highly Efficient Gradient Boosting Decision Tree*. Retrieved January 27, 2026, from https://github.com/Microsoft/LightGBM.

Kuras, A., Brell, M., Rizzi, J., & Burud, I. (2021). Hyperspectral and Lidar Data Applied to the Urban Land Cover Machine Learning and Neural-Network-Based Classification: A Review. *Remote Sensing 2021, Vol. 13, 13*(17). https://doi.org/10.3390/RS13173393

Labetski, A., Vitalis, S., Biljecki, F., Arroyo Ohori, K., & Stoter, J. (2023a). 3D building metrics for urban morphology. *International Journal of Geographical Information Science*, *37*(1), 36–67. https://doi.org/10.1080/13658816.2022.2103818

Labetski, A., Vitalis, S., Biljecki, F., Arroyo Ohori, K., & Stoter, J. (2023b). 3D building metrics for urban morphology. *International Journal of Geographical Information Science*, *37*(1), 36–67. https://doi.org/10.1080/13658816.2022.2103818

Li, Z. L., Tang, B. H., Wu, H., Ren, H., Yan, G., Wan, Z., Trigo, I. F., & Sobrino, J. A. (2013). Satellite-derived land surface temperature: Current status and perspectives. *Remote Sensing of Environment*, *131*, 14–37. https://doi.org/10.1016/J.RSE.2012.12.008

Matias, M., & Lopes, A. (2024). LCZ thermal and exoatmospheric albedo assessment using Landsat 8 land surface temperature and reflectance dataset: Case study of Lisbon. *Remote Sensing Applications: Society and Environment*, *34*. https://doi.org/10.1016/J.RSASE.2024.101163

Melesse, A. M., Weng, Q., Thenkabail, P. S., & Senay, G. B. (2007). Remote sensing sensors and applications in environmental resources mapping and modelling. *Sensors*, *7*(12), 3209–3241. https://doi.org/10.3390/S7123209

Meng, Q., Zhang, L., Sun, Z., Meng, F., Wang, L., & Sun, Y. (2018). Characterizing spatial and temporal trends of surface urban heat island effect in an urban main built-up area: A 12-year case study in Beijing, China. *Remote Sensing of Environment*, *204*, 826–837. https://doi.org/10.1016/J.RSE.2017.09.019

Molua, C. O., & Ataman, J. O. (2024a). Applications of Lidar Technology in Urban Geophysical Surveys. *International Journal of Information Technology and Computer Engineering*, (44), 47–58. https://doi.org/10.55529/IJITC.44.47.58

Molua, C. O., & Ataman, J. O. (2024b). Applications of Lidar Technology in Urban Geophysical Surveys. *International Journal of Information Technology and Computer Engineering*, (44), 47–58. https://doi.org/10.55529/IJITC.44.47.58

Niu, L., Zhang, Z., Peng, Z., Liang, Y., Liu, M., Jiang, Y., Wei, J., & Tang, R. (2021). Identifying Surface Urban Heat Island Drivers and Their Spatial Heterogeneity in China's 281 Cities: An Empirical Study Based on Multiscale Geographically Weighted Regression. *Remote Sensing 2021, Vol. 13, 13*(21). https://doi.org/10.3390/RS13214428

Oke, T. R. (1982). The energetic basis of the urban heat island. *Quarterly Journal of the Royal Meteorological Society*, *108*(455), 1–24. https://doi.org/10.1002/QJ.49710845502

Oke, T. R. (2002). Boundary Layer Climates. *Boundary Layer Climates*. https://doi.org/10.4324/9780203407219

Oke, T. R., Mills, G., Christen, A., & Voogt, J. A. (2017). Urban Heat Island. *Urban Climates*, 197–237. https://doi.org/10.1017/9781139016476.008

Oliveira, A., Lopes, A., Correia, E., Niza, S., & Soares, A. (2021). Heatwaves and Summer Urban Heat Islands: A Daily Cycle Approach to Unveil the Urban Thermal Signal Changes in Lisbon, Portugal. *Atmosphere 2021, Vol. 12, 12*(3). https://doi.org/10.3390/ATMOS12030292

Park, J., Kim, J. H., Lee, D. K., Park, C. Y., & Jeong, S. G. (2017). The influence of small green space type and structure at the street level on urban heat island mitigation. *Urban Forestry and Urban Greening*, *21*, 203–212. https://doi.org/10.1016/J.UFUG.2016.12.005

Peel, M. C., Finlayson, B. L., & McMahon, T. A. (2007). Updated world map of the Köppen-Geiger climate classification. *Hydrology and Earth System Sciences*, *11*(5), 1633–1644. https://doi.org/10.5194/hess-11-1633-2007

Ren, C., Ng, E. Y. Y., & Katzschner, L. (2011a). Urban climatic map studies: A review. *International Journal of Climatology*, *31*(15), 2213–2233. https://doi.org/10.1002/JOC.2237

Ren, C., Ng, E. Y. Y., & Katzschner, L. (2011b). Urban climatic map studies: A review. *International Journal of Climatology*, *31*(15), 2213–2233. https://doi.org/10.1002/JOC.2237;PAGE:STRING:ARTICLE/CHAPTER

Roth, M. (2007). Review of urban climate research in (sub)tropical regions. *International Journal of Climatology*, *27*(14), 1859–1873. https://doi.org/10.1002/JOC.1591

Rozenstein, O., Qin, Z., Derimian, Y., & Karnieli, A. (2014). Derivation of land surface temperature for landsat-8 TIRS using a split window algorithm. *Sensors (Switzerland)*, *14*(4), 5768–5780. https://doi.org/10.3390/S140405768

Salazar Miranda, A., Du, G., Gorman, C., Duarte, F., Fajardo, W., & Ratti, C. (2022). Favelas 4D: Scalable methods for morphology analysis of informal settlements

using terrestrial laser scanning data. *Environment and Planning B: Urban Analytics and City Science*, *49*(9), 2345–2362. https://doi.org/10.1177/23998083221080174;WGROUP:STRING:PUBLICATION

Schwarz, N., Lautenbach, S., & Seppelt, R. (2011). Exploring indicators for quantifying surface urban heat islands of European cities with MODIS land surface temperatures. *Remote Sensing of Environment*, *115*(12), 3175–3186. https://doi.org/10.1016/J.RSE.2011.07.003

Shi, T., Chen, M., Li, J., & Lu, G. (2025). Quantifying the driving force of urban morphologies on canopy urban heat island: a machine learning approach with educational application. *Frontiers in Environmental Science*, *13*, 1647596. https://doi.org/10.3389/FENVS.2025.1647596/BIBTEX

Silva, R., Carvalho, A. C., Pereira, S. C., Carvalho, D., & Rocha, A. (2022). Lisbon urban heat island in future urban and climate scenarios. *Urban Climate*, *44*. https://doi.org/10.1016/J.UCLIM.2022.101218

Sobrino, J. A., Jiménez-Muñoz, J. C., & Paolini, L. (2004). Land surface temperature retrieval from LANDSAT TM 5. *Remote Sensing of Environment*, *90*(4), 434–440. https://doi.org/10.1016/J.RSE.2004.02.003

Sobrino, J. A., Oltra-Carrió, R., Sòria, G., Jiménez-Muñoz, J. C., Franch, B., Hidalgo, V., Mattar, C., Julien, Y., Cuenca, J., Romaguera, M., Gómez, J. A., de Miguel, E., Bianchi, R., & Paganini, M. (2013). Evaluation of the surface urban heat island effect in the city of Madrid by thermal remote sensing. *International Journal of Remote Sensing*, *34*(9–10), 3177–3192. https://doi.org/10.1080/01431161.2012.716548

Stewart, I. D., & Oke, T. R. (2012). Local climate zones for urban temperature studies. *Bulletin of the American Meteorological Society*, *93*(12), 1879–1900. https://doi.org/10.1175/BAMS-D-11-00019.1

Streutker, D. R. (2002). A remote sensing study of the urban heat island of Houston, Texas. *International Journal of Remote Sensing*, *23*(13), 2595–2608. https://doi.org/10.1080/01431160110115023

Sukma, A. I., Koeva, M. N., Reckien, D., Bockarjova, M., da Silva Mano, A., Canili, G., Vicentini, G., & Kerle, N. (2024). 3D City Digital Twin Simulation to Mitigate Heat Risk of Urban Heat Islands. *The International Archives of the Photogrammetry, Remote Sensing and Spatial Information Sciences*, *XLVIII-4-W11-2024*(4/W11-2024), 129–136. https://doi.org/10.5194/ISPRS-ARCHIVES-XLVIII-4-W11-2024-129-2024

Tanoori, G., Soltani, A., & Modiri, A. (2024). Machine Learning for Urban Heat Island (UHI) Analysis: Predicting Land Surface Temperature (LST) in Urban Environments. *Urban Climate*, *55*, 101962. https://doi.org/10.1016/J.UCLIM.2024.101962

Tardy, B., Rivalland, V., Huc, M., Hagolle, O., Marcq, S., & Boulet, G. (2016). A software tool for atmospheric correction and surface temperature estimation of Landsat infrared thermal data. *Remote Sensing*, *8*(9). https://doi.org/10.3390/RS8090696

Voogt, J. A., & Oke, T. R. (2003). Thermal remote sensing of urban climates. *Remote Sensing of Environment*, *86*(3), 370–384. https://doi.org/10.1016/S0034-4257(03)00079-8

Wang, R., Ren, C., Xu, Y., Lau, K. K. L., & Shi, Y. (2018). Mapping the local climate zones of urban areas by GIS-based and WUDAPT methods: A case study of Hong Kong. *Urban Climate*, *24*, 567–576. https://doi.org/10.1016/J.UCLIM.2017.10.001

Wehr, A., & Lohr, U. (1999). Airborne laser scanning - An introduction and overview. *ISPRS Journal of Photogrammetry and Remote Sensing*, *54*(2–3), 68–82. https://doi.org/10.1016/S0924-2716(99)00011-8

Weng, Q. (2009). Thermal infrared remote sensing for urban climate and environmental studies: Methods, applications, and trends. *ISPRS Journal of Photogrammetry and Remote Sensing*, *64*(4), 335–344. https://doi.org/10.1016/J.ISPRSJPRS.2009.03.007

Xu, Y., Ren, C., Ma, P., Ho, J., Wang, W., Lau, K. K. L., Lin, H., & Ng, E. (2017a). Urban morphology detection and computation for urban climate research. *Landscape and Urban Planning*, *167*, 212–224. https://doi.org/10.1016/J.LANDURBPLAN.2017.06.018

Xu, Y., Ren, C., Ma, P., Ho, J., Wang, W., Lau, K. K. L., Lin, H., & Ng, E. (2017b). Urban morphology detection and computation for urban climate research. *Landscape and Urban Planning*, *167*, 212–224. https://doi.org/10.1016/J.LANDURBPLAN.2017.06.018

Xu, Y., Ren, C., Ma, P., Ho, J., Wang, W., Lau, K. K. L., Lin, H., & Ng, E. (2017c). Urban morphology detection and computation for urban climate research. *Landscape and Urban Planning*, *167*, 212–224. https://doi.org/10.1016/J.LANDURBPLAN.2017.06.018

Yan, W. Y., Shaker, A., & El-Ashmawy, N. (2015a). Urban land cover classification using airborne LiDAR data: A review. *Remote Sensing of Environment*, *158*, 295–310. https://doi.org/10.1016/J.RSE.2014.11.001

Yan, W. Y., Shaker, A., & El-Ashmawy, N. (2015b). Urban land cover classification using airborne LiDAR data: A review. *Remote Sensing of Environment*, *158*, 295–310. https://doi.org/10.1016/J.RSE.2014.11.001

Yuan, Q. (n.d.). *Urban Land-use Features Mapping from LiDAR and Remote Sensing Images using Visual Transformer Network Model*. https://doi.org/10.5194/isprs-archives-XLVIII-M-5-2024-195-2025

Zhang, Y., Ge, J., Wang, S., & Dong, C. (2025). Optimizing urban green space configurations for enhanced heat island mitigation: A geographically weighted machine learning approach. *Sustainable Cities and Society*, *119*, 106087. https://doi.org/10.1016/J.SCS.2024.106087

Zhao, C., Jensen, J., Weng, Q., Currit, N., & Weaver, R. (2019). Application of airborne remote sensing data on mapping local climate zones: Cases of three metropolitan areas of Texas, U.S. *Computers, Environment and Urban Systems*, *74*, 175–193. https://doi.org/10.1016/J.COMPENVURBSYS.2018.11.002

Zhou, D., Xiao, J., Bonafoni, S., Berger, C., Deilami, K., Zhou, Y., Frolking, S., Yao, R., Qiao, Z., & Sobrino, J. A. (2018). Satellite Remote Sensing of Surface Urban Heat Islands: Progress, Challenges, and Perspectives. *Remote Sensing 2019, Vol. 11, 11*(1). https://doi.org/10.3390/RS11010048

Zhou, D., Zhao, S., Zhang, L., & Liu, S. (2016). Remotely sensed assessment of urbanization effects on vegetation phenology in China's 32 major cities. *Remote Sensing of Environment*, *176*, 272–281. https://doi.org/10.1016/j.rse.2016.02.010

APPENDIX

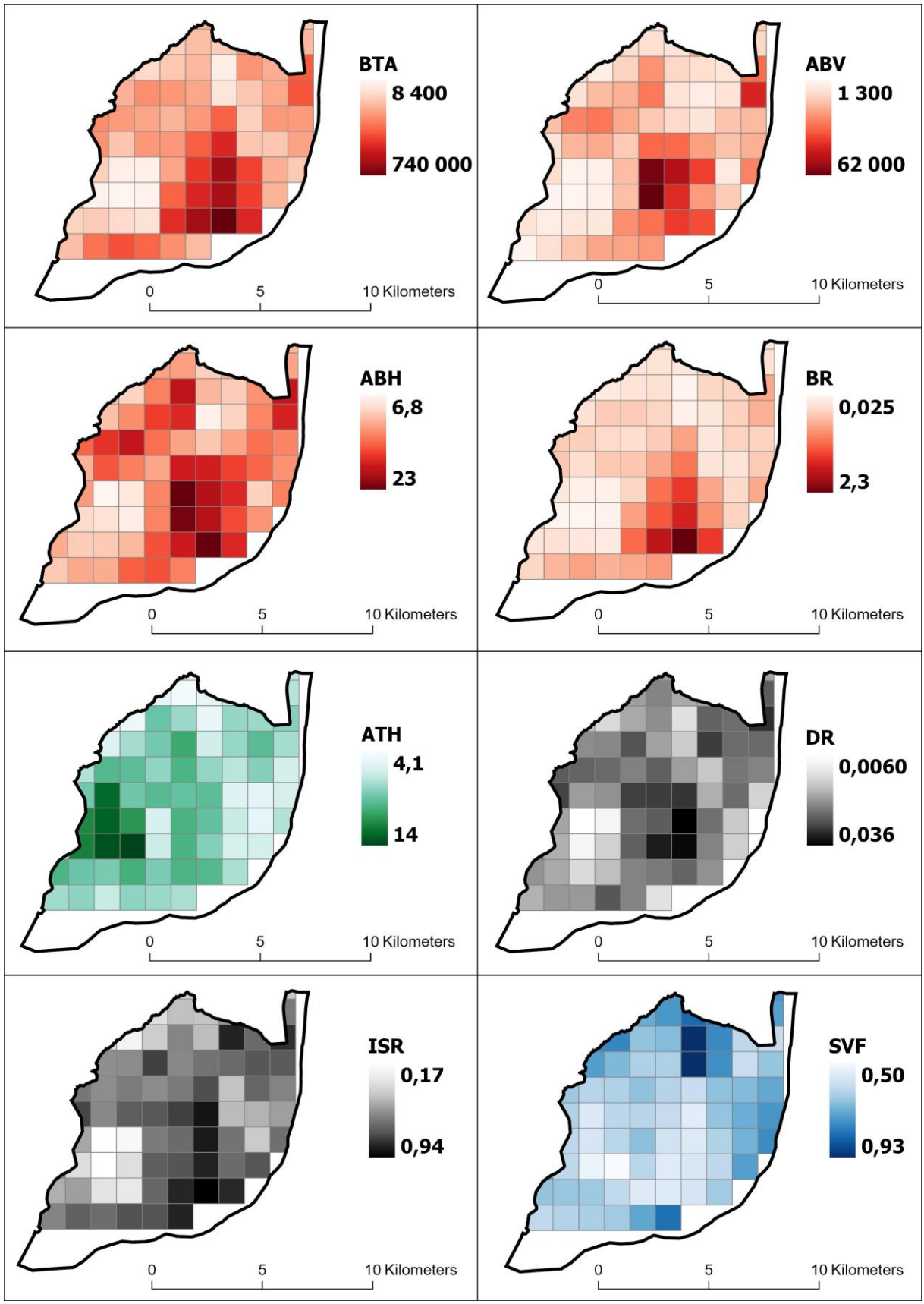

Appendix 1 : Spatial distribution of morphological indicators in the study region

Masters Program in **Geospatial Technologies**

Supported by:
Education and Culture
ERASMUS MUNDUS